

Frontal Polymerization in Microgravity
Summary of Research
Dr. John A. Pojman
Department of Chemistry and Biochemistry
2/1/98 - 12/31/02
University of Southern Mississippi, Box 5157, Hattiesburg, MS 39406
NAG8-1466

Abstract

The project began with frontal polymerization (FP). We studied many aspects of FP on the ground and performed two successful weeks of flying on the KC-135. The project evolved into the current flight investigation, Transient Interfacial Phenomena in Miscible Polymer Systems (TIPMPS, as we recognized that an essential question could best be studied using a non-frontal approach. We present detailed results from our ground-based work on FP, KC-135 results and the background, justification and numerical work for the TIPMPS project.

Co-Investigators:

Volpert, V.A.
Universite Lyon I

Wilke, H.
Institute of Crystal Growth, Berlin

Introduction

The project began in February 1998 with the goal to answer these six questions.

- 1) How does surface-tension induced convection (STIC) affect frontal polymerization?
- 2) How does buoyancy-driven convection affect the "hydrodynamic instability"?
- 3) How do bubbles interact with fronts?
- 4) How does STIC affect spin modes?
- 5) How does convection affect frontal polymerization with a solid monomer?

6) What is the effect of gravity on phase separation in frontal polymerization?

We now briefly explain frontal polymerization:

Frontal polymerization is a mode of converting monomer into polymer via a localized reaction zone that propagates, most often through the coupling of thermal diffusion and Arrhenius reaction kinetics. Frontal polymerization reactions were first discovered in Russia by Chechilo and Enikolopyan in 1972.¹ They studied methyl methacrylate polymerization to determine the effect of initiator type and concentration on front velocity² and the effect of pressure.³ A great deal of work on the theory of frontal polymerization was performed.⁴⁻⁹ Work was also done with epoxy curing.¹⁰

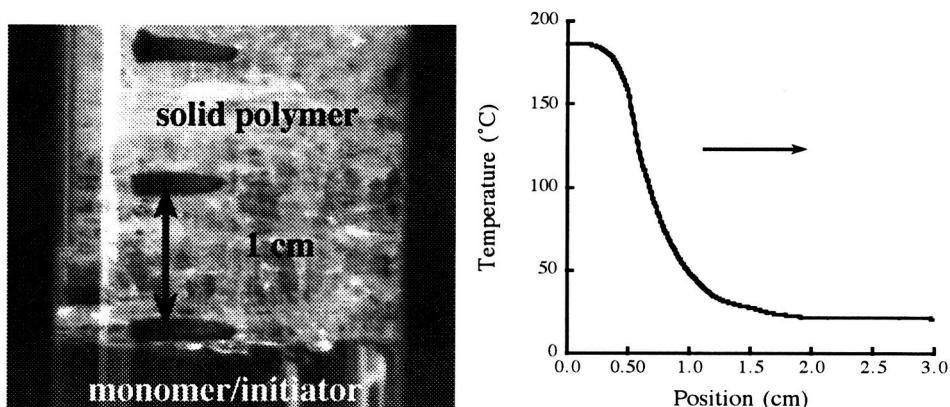


Figure 1. Left: A descending case of frontal polymerization with triethylene glycol dimethacrylate and benzoyl peroxide as the initiator. Right: The temperature profile for a benzyl acrylate front, with ultrafine silica gel added to prevent convection.

Pojman and his co-workers demonstrated the feasibility of traveling fronts in solutions of thermal free-radical initiators in a variety of neat monomers at ambient pressure using liquid monomers that form polymers with melting points exceeding the reaction temperature of the front¹¹⁻¹³ and with a solid monomer.¹⁴ The macrokinetics and dynamics of frontal polymerization have been examined in detail¹⁵ and applications for materials synthesis considered.¹⁶

Basic Phenomena

Frontal polymerization reactions are relatively easy to perform. In the simplest case, a test tube is filled with the initial reactions. The front is ignited by applying heat to one end of the tube with an electric heater. The position of the front is obvious because of the difference in the optical properties of polymer and monomer. The velocity can be affected by the initiator type and concentration but is on the order of a cm/min.

The defining features of frontal polymerization are the sharp temperature and concentration gradients present in the front. Figure 1 shows a temperature profile for benzyl acrylate polymerization. Notice that the temperature jumps about 100 °C over 1 cm. The concentration gradient is two orders of magnitude larger.

We describe cases when frontal polymerization can be observed (descending fronts) under moderate pressures (<5 atm). The first case is crosslinking monomers (thermosets), including tri(ethylene glycol)dimethacrylate (TGDMA), di(ethylene glycol)dimethacrylate (DGDMA), and divinylbenzene. The free-radical polymerization of these monomers produces rigid crosslinked polymers, which sustain a sharp frontal interface (see Figure 1).

The second group of monomers form polymers that are insoluble in the monomer. Good examples are acrylic and methacrylic acids.^{11, 13, 17} Insoluble polymer particles adhere to each other during their formation and stick to the reactor or test tube walls, forming a mechanically durable phase and discernible polymer-monomer interface.

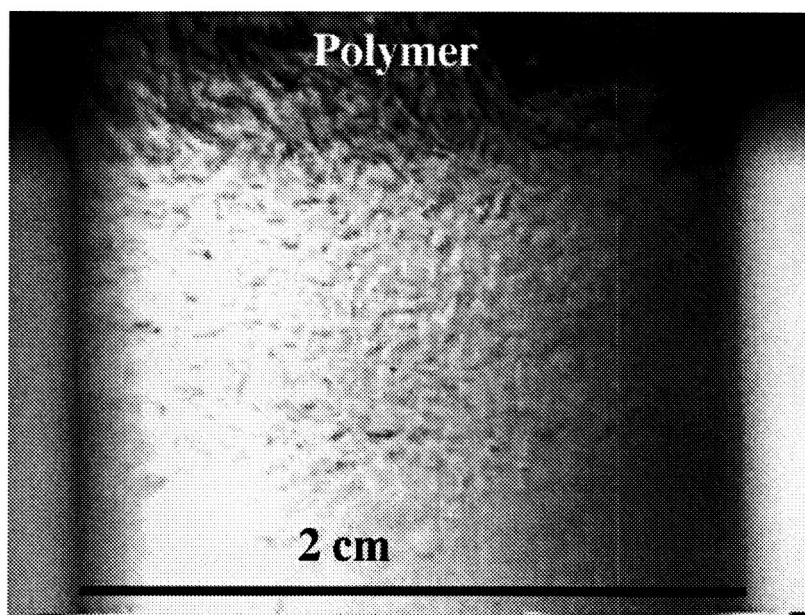


Figure 2. Rayleigh-Taylor instability with descending front of butyl acrylate polymerization. Although the polymer product is hot (> 200 °C) it still is about 20% more dense than the monomer below it.

The third group of monomers includes all highly reactive monomers that produce thermoplastic polymers, which are molten at the front temperature. Such fronts decay due to the Rayleigh-Taylor instability (Figure 2). Although these polymers are soluble in their monomers (given sufficient time), on the time scale of the front the polymer is effectively immiscible with the monomer. Adding an inert filler such as ultra-fine silica gel (Cabosil) increases the viscosity and eliminates the front collapse. However, adding a filler prevents the production of a homogeneous product. Some monomers like styrene and methyl methacrylate require moderate pressure (20-30 atm) to eliminate monomer boiling. Higher boiling temperature monomers like

butyl methacrylate, butyl acrylate and benzyl acrylate support the frontal regime at ambient pressure in test tubes.

In the early work on frontal polymerization, the authors^{1-3, 18} applied very high pressure (up to 5000 atm) to eliminate monomer (methyl methacrylate) boiling and the reaction zone decay due to the density gradient in the reaction zone (Rayleigh-Taylor instability) caused by the more dense polymer product overlying the unreacted monomer. They also managed to observe only downward traveling fronts because natural convection rapidly removed heat from the reaction zone of an ascending front leading to extinction. However, at pressures less than 1500 atm descending fronts decayed.

Because of the large thermal and concentration gradients, polymerization fronts are highly susceptible to buoyancy-induced convection. Garbey et al. performed the linear stability analysis for the liquid/liquid and liquid/solid cases.¹⁹⁻²¹ The bifurcation parameter was a 'frontal Rayleigh number':

$$R = g\beta q\kappa^2/\nu c^3 \quad (1)$$

where g is the gravitational acceleration, b the thermal expansion coefficient, q the temperature increase at the front, k the thermal diffusivity, n the kinematic viscosity and c the front velocity.

Let us first consider the liquid/solid case. Neglecting heat loss, the descending front is always stable because it corresponds to heating a fluid from above. The front is always flat. If the front is ascending, convection may occur depending on the parameters of the system.

Bowden et al. experimentally confirmed that the first mode is an antisymmetric one, followed by an axisymmetric one.²² Figure 3 shows a flat descending front as well as axisymmetric and antisymmetric modes of ascending fronts. Figure 3 shows the stability diagram in the viscosity-front velocity plane. Most importantly, they confirmed that the stability of the fluid was a function not only of the viscosity but also of the front velocity. This means that the front dynamics affects the fluids dynamics, unlike with pH fronts and chemical waves in the BZ reaction in which the front velocity does not play a role in the stability of the fluid.²³⁻²⁸

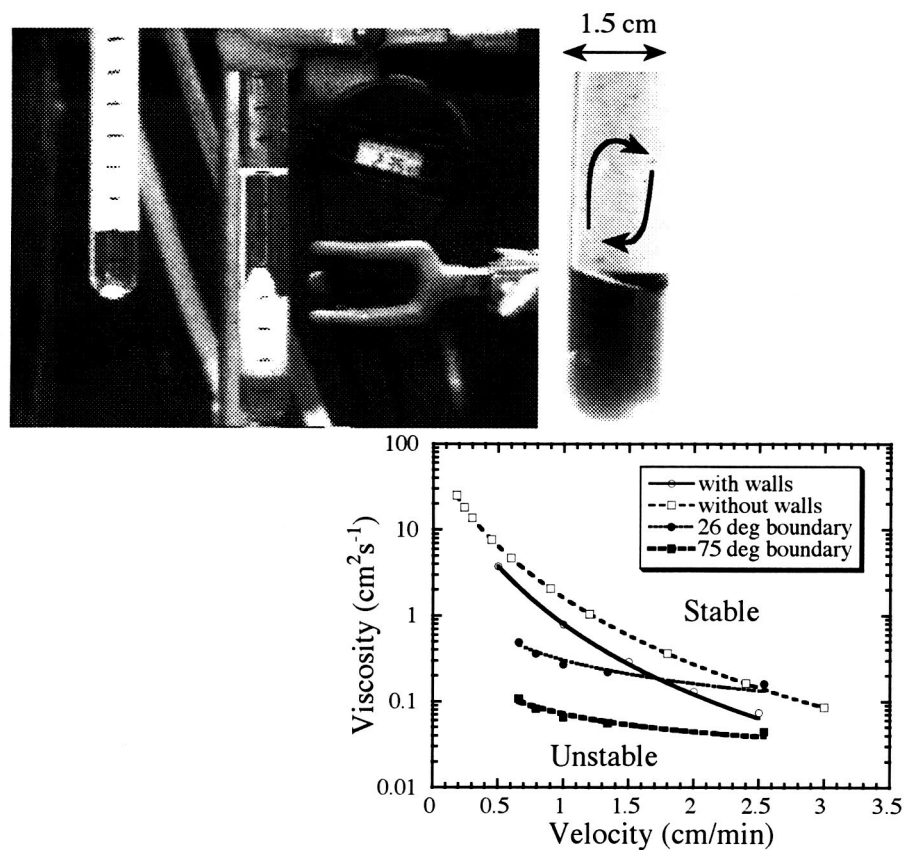


Figure 3. Left: The front on the left is descending and the one on the right ascending with an axisymmetric mode of convection. Right: An antisymmetric mode of an ascending front. The system is the acrylamid/bis-acrylamide polymerization in DMSO with persulfate initiator. The stability diagram for the system. From Bowden et al.²²

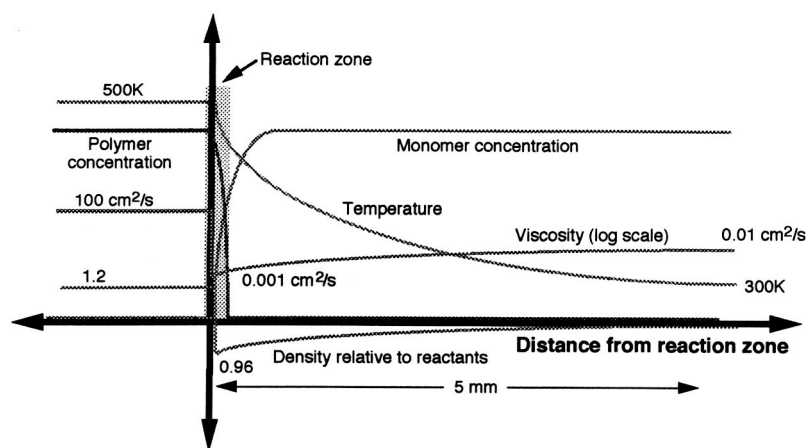


Figure 4. Schematic diagram showing changes in properties across a propagating polymerization front. (Courtesy of Paul Ronney.)

Liquid/liquid systems are more complicated than the previous case because a descending front can exhibit the Rayleigh-Taylor instability. Consider the schematic in Figure 4. The product is hotter than the reactant but is more dense, and because the product is a liquid, fingering can occur. Such front degeneration is shown in Figure 2. The Rayleigh-Taylor instability can be overcome using high pressure¹, adding a filler,²⁹ using a dispersion in salt water³⁰ or performing the fronts in weightlessness.³⁰

McCaughey et al. tested the analysis of Garbey et al. and found the same bifurcation sequence of antisymmetric to axisymmetric convection in ascending fronts³¹ as seen with the liquid/solid case.

Effect of Gravity on Frontal Polymerization

In 1998 and 1999 we focused on the effect of gravity on frontal polymerization. We studied ascending fronts of thermosets in which gradients of composition were prepared by pumping the reactants in from the top with two pumps.^{32,33} We have shown that buoyancy-driven convection plays a major role in gradient formation in ascending fronts with a solid product.³⁴

Orientation

We observed that the velocities of descending thermoset polymerization fronts were strongly affected by the orientation of the tube.³⁵ The front remained approximately perpendicular to the gravitational vector but propagated almost 1.8 times as fast at 75° along the axis of the tube. We performed a study of the velocity and front shape dependence on orientation using propagating fronts of triethylene glycol dimethacrylate with peroxide initiator and acrylamide/bisacrylamide polymerization in DMSO with persulfate initiator. The percentage increase of velocity was independent of the initiator concentration but strongly dependent on the viscosity. Convection under the front flowed away from the tube wall nearest the vertical axis and was stronger as the angle was increased. The front shape also changed, becoming significantly distorted near the wall from which the convection originated (Figure 5). We applied a simple geometric argument to explain the angular dependence for small angles based on the assumption that convection did not affect the velocity of propagation normal to the front (Figure 6). The increase in velocity along the tube axis could be explained by a projection of the normal velocity onto the tube axis, following a $1/\cos\theta$ dependence. For higher angles, the convection was not sufficiently strong to maintain a level front. When the difference from a 180° orientation was taken into account, the velocity dependence exactly followed the geometric relationship (Figure 7).

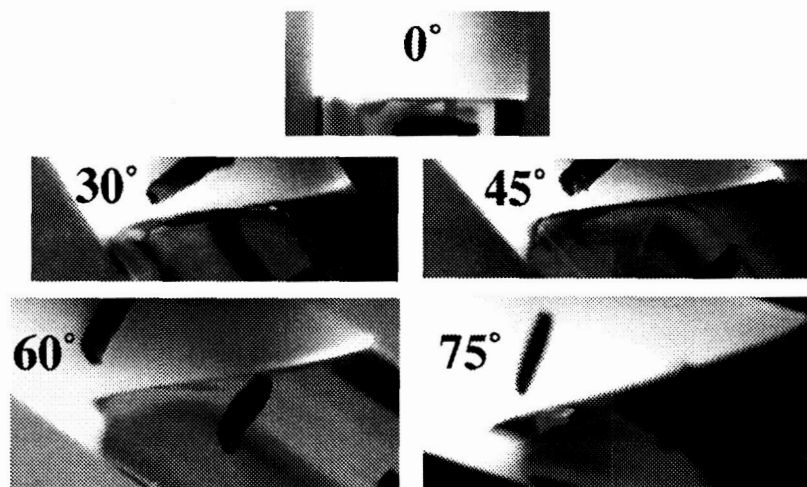


Figure 5. The effect of orientation on descending fronts of acrylamide in polymerization DMSO fronts.

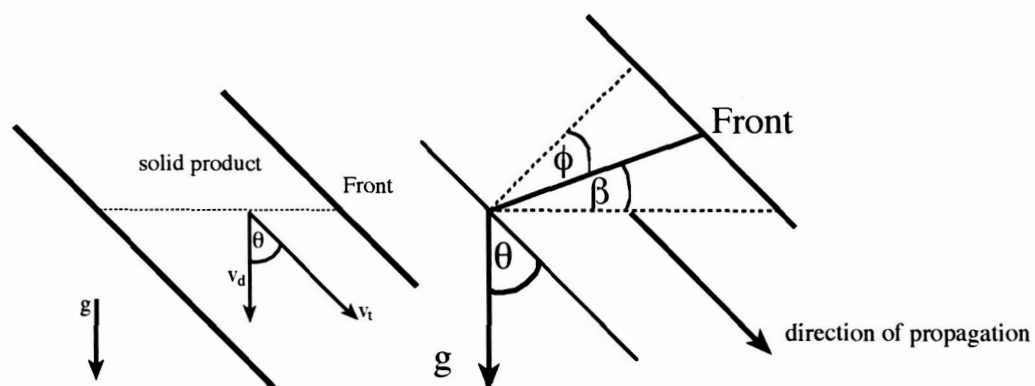


Figure 6. Left: Geometry of front propagation in a tilted tube. Right: The actual front angle with the respect to the horizontal, β , must be subtracted from θ to yield the corrected, or effective angle of, ϕ .

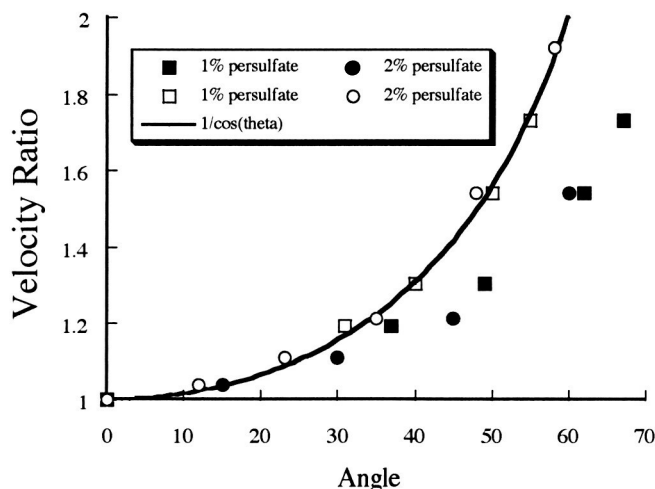


Figure 7. Velocity ratio (between the measured value and the 0° case) versus angle for descending front of acrylamide polymerization in DMSO with persulfate initiator. Solid markers are for uncorrected angles (θ). Open markers correspond to corrected angles ($\theta - \phi$).

Thermal Instabilities

Fronts do not have to propagate as simple planar fronts. Analogously to oscillating reactions, a steady state can lose its stability as a parameter is varied and exhibit periodic behavior, either as pulsations or ‘spin modes’ in which a hot spot propagates around the reactor as the front propagates, leaving a helical pattern. This mode was first observed in Self-propagating High temperature Synthesis (SHS).³⁶

The linear stability analysis of the longitudinally propagating fronts in the cylindrical adiabatic reactors with one overall reaction predicted that the expected frontal mode for the given reactive medium and diameter of reactor is governed by the Zeldovich number:

$$Z = \frac{T_m - T_0}{T_m} \frac{E_{eff}}{RT_m} \quad (2)$$

For FP, lowering the initial temperature (T_0), increasing the front temperature (T_m), increasing the energy of activation (E_{eff}) all increase the Zeldovich number. The planar mode is stable if $Z < Z_{cr} = 8.4$, and unstable if $Z > Z_{cr}$. By varying the Zeldovich number beyond the stability threshold, subsequent bifurcations leading to higher spin mode instabilities can be observed. Secondly, for a cylindrical geometry the number of spin heads or hot spots is also a function of the tube diameter. We point out that polymerization is not a one-step reaction, so that the above form of the Zeldovich number does not directly apply. However, estimates of the effective Zeldovich number can be obtained from estimates with the steady-state assumption for free-radical polymerization.

The most commonly observed case with frontal polymerization is the spin mode in which a ‘hot spot’ propagates around the front. A helical pattern is often observed in the sample. The first case was with the frontal polymerization of ϵ -caprolactam,^{37, 38} and the next case was

discovered by Pojman et al. in the methacrylic acid system in which the initial temperature was lowered.³⁹

The single-head spin mode was studied in detail by Ilyashenko and Pojman.⁴⁰ They were able to estimate the Zeldovich number using kinetic parameters for the initiator and the methacrylic acid. The value at room temperature was about 7, less than the critical value for spin modes. In fact, fronts at room temperature were planar and spin modes only appeared by lowering the initial temperature. However, spin modes could be observed by increasing the heat loss from the reactor by immersing the tube in water or oil. The simple analysis assumes an adiabatic system.

Effect of Convection

The physical mechanism leading to appearance of the spinning modes for polymerization fronts is the same as for combustion fronts. However, if the polymer or the monomer is in the liquid phase, then the properties of these regimes and the critical values of parameters when they appear can be influenced by hydrodynamics.

Consider a polymerization front with a liquid monomer and a solid polymer propagating upwards. If the Zeldovich number is sufficiently large, then the planar reaction front loses its stability resulting in appearance of a spinning mode. The high-temperature spots formed near the reaction front can lead to a convective motion of the liquid monomer above the front. This motion will mix the hot monomer near the front with the cold monomer above the front and, consequently, will decrease the temperature at the high-temperature spot. Therefore convection acts against the thermal instability, and the critical value of the Zeldovich number increases with increase of the Rayleigh number.¹⁹ In other words, there are two bifurcation parameters needed to describe the appearance of spin modes – the Zeldovich number and the frontal Rayleigh number.

If the front propagates downwards, the convective motion decreases the heat loss from the high-temperature spot to the unreacted monomer. The heat is conserved near the reaction front, and the perturbation of the temperature has better conditions to increase. Hence the critical value of the Zeldovich number decreases. We note that the influence of convection on the spinning modes for polymerization fronts with a liquid polymer is different in comparison with the case of a solid polymer.²¹

We provided the first experimental confirmation that gravity plays a role in spin modes in a liquid/solid system came in the study of descending fronts in which the viscosity was significantly increased with silica gel.⁴¹ Masere et al. found that silica gel significantly altered the spin behavior. Pojman et al. made a similar observation in square reactors.⁴²

New Initiator

Because peroxides and nitriles produce volatile products, bubbles are formed in frontal polymerization. We developed a bubble-free, organic soluble initiator, a tetra-alkylammonium persulfate, which allows the study of frontal polymerization at ambient pressure.⁴³

Interfacial effects on frontal polymerization

We developed a model to study the Marangoni instability in a propagating front. Using parameters applicable to FP, we have demonstrated analytically that a Marangoni instability can occur. Numerical simulations confirmed this.⁴⁴

KC-135 flights

We performed two KC-135 flights: February 1999 and February 2000. We provide the following highlights.

Confirmation of orientation effect. Using triethylene glycol dimethacrylate fronts, we observed how a tilted front recovered during weightlessness. Figure 8 shows a front. Because of the short time of the weightlessness, it was not possible to observe complete relaxation of the front to a plane front perpendicular to the axis of the tube.

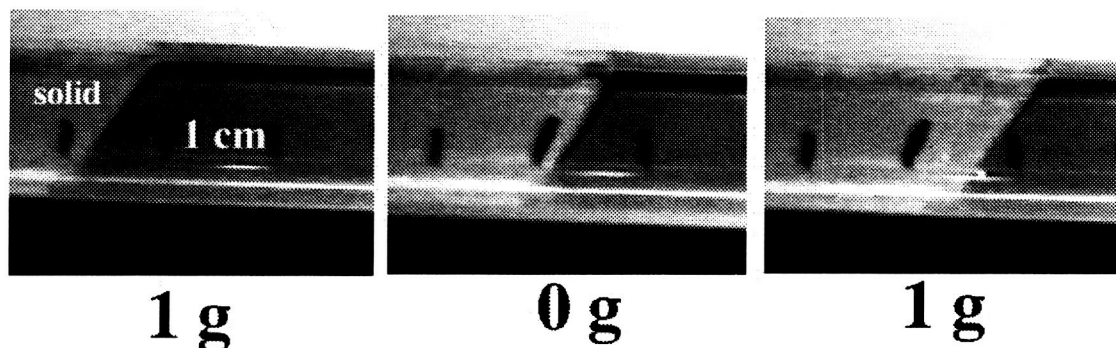


Figure 8. Front of TGMDA in a tube that was initially at 45° with respect to gravity.

Microporous Foams with Methacrylic Acid

Pojman et al. found an unusual mode of propagation when there are large amounts of bubbles.³⁹ In studying fronts of methacrylic acid polymerization, they observed convection that periodically occurred under the front at the same time as the front deformed and undulated. The period of convection was about 20 seconds and remained constant during the entire front propagation.

Volpert et al. have analyzed the effect the thermal expansion of the monomer on the thermal stability and concluded that the reaction front becomes less stable than without thermal expansion⁴⁵. The effective thermal expansion can be increased because of the bubbles, and it can considerably affect the stability conditions. We were able to observe the Darius-Landau Instability with methacrylic acid. The distortion to the front increased in low g, indicating that buoyancy-driven convection dampens the instability (Figure 9).

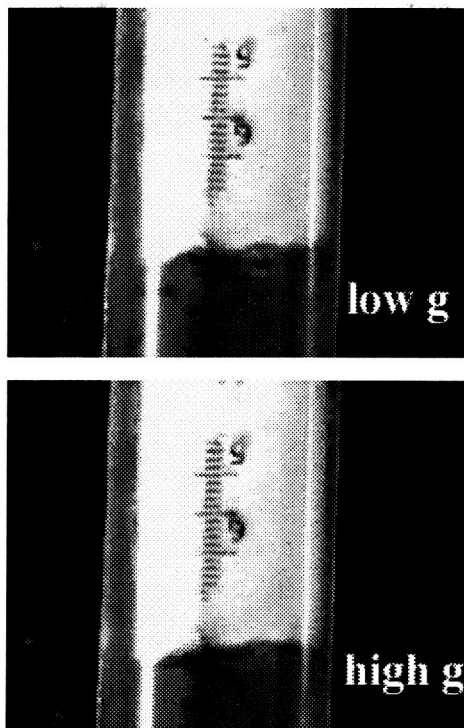


Figure 9. The shape of the front with methacrylic acid changes with differences in g level.

Attempts to Observe Convection in mg

With the frontal polymerization of hexyl acrylate we attempted to observe convection caused by the supposed gradient of effective interfacial tension (see below for further discussion). It was not possible to initiate the front and observe propagation in 20 seconds. Also, bubbles appeared from dissolved air. Figure 10 shows two images separated by a few seconds showing how g jitter mixed the system, preventing any clear observation of convection.

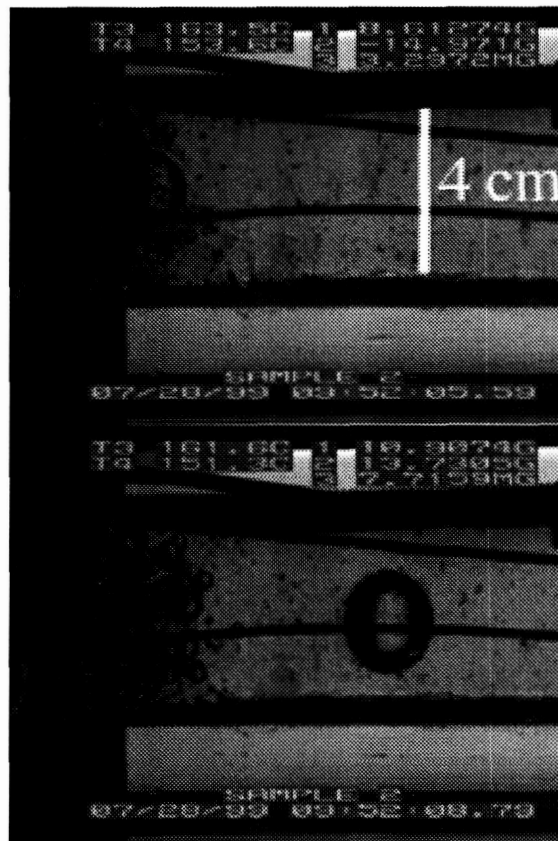


Figure 10. Two images of a hexyl acrylate polymerization front in the low g phase of the parabola. Notice how the bubble has moved to the right (down).

Observations of glycerin and water in low g

We observed the behavior of glycerin in water and water in glycerin to determine if drops change their shape as would two immiscible fluids. In Figure 11 we see a drop of water in glycerin. It does not assume a spherical shape as would be expected if an interfacial tension were acting as with immiscible fluids. The drop does become spherical but only we the acceleration level begins to increase.

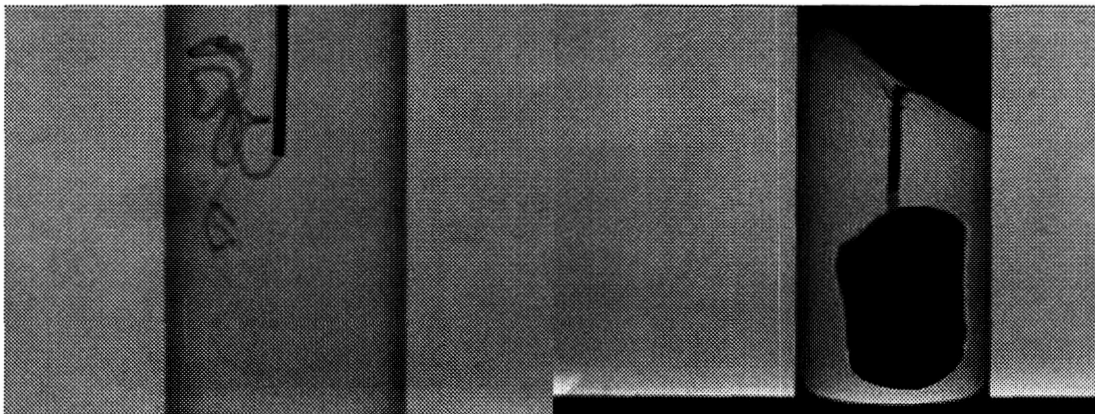


Figure 11. Left: Glycerin (with dye) injected into water in weightlessness. Right: Water (with dye) injected into glycerin in weightlessness. Tube diameter in both cases is 2.2 cm.

In Figure 11 we see glycerin injected into water. It did not form into a drop because the viscosity of water is 1/1000 that of glycerin. The stream of glycerin did not break up into droplets indicating either that the effective interfacial tension is too weak to have an effect during the few seconds available for observation or that the effective interfacial tension does not cause behavior as seen with immiscible fluids.

Frontal Foams

Polymeric foams are a very important class of materials. They serve a wide variety of purposes from the insulation of refrigerators, the packaging of foods, and padding of chairs to the construction of lightweight but durable building materials.⁴⁶ Commercial production of polymeric foams was first introduced more than fifty years ago, and since that time much work has been carried out in an effort to improve the current production methods in order to produce foams with specific properties suitable for specific environments.⁴⁷ With the emergence of new technologies and production techniques, it is now possible to produce a polymer foam using almost any polymeric material.⁴⁸

Wessling et al. reported the first polyurethane foam produced in reduced gravity in which they found major differences in the foam and cell structures formed, compared to those formed on Earth.^{49, 50} Bergman proposed that the space-based production of foams would prevent imperfections in the finished product caused by cell drainage and sedimentation.⁵¹ Curtin et al. sought to produce high quality foams in reduced gravity, free of defects in order to test heat transfer theories and for uses as a standard reference material.⁵²

Studies have been carried out under reduced gravity to determine the effects of gravity on the properties of foams produced through other methods.^{50, 52} These experiments found that gravity can have significant effects on the size and shape of cells formed, the density of the foam produced, and distribution of the cells within the polymer.

We sought to develop a relatively simple method for the production of polymeric foams that does not require mixing or continuous heating. Frontal polymerization offers this possibility. We undertook the first stages of developing this technology using the simplest systems possible. Because no surfactant or nucleating agents were employed, large bubbles formed, unlike commercial foams. However, the systems used provide information on how bubbles affect frontal polymerization and are affected by it.

Bubble interactions in frontal polymerization reactions were studied by Pojman et al. on the *Conquest I* sounding rocket with n-butyl acrylate⁵³ and were followed by a series of KC-135 parabolic flights studying thermosets.^{54, 56} They reported evidence of unusual bubble interactions in reduced gravity. In the *Conquest I* sample, they observed a periodic pattern of bubbles “connected like a necklace” with a region of polymer followed by a large bubble, followed by another region of polymer.

Because the video failed on the rocket flight, it was not possible to determine if the periodic structure resulted from a periodic mode of propagation or because of a thermodynamically-driven aggregation after the front. The periodicity could have arisen from a large bubble pinching off to minimize the free energy. However, there is precedent in frontal polymerization

for periodic propagation modes. The expansion of poly(methacrylic acid) in a front, caused by gas from the initiator, was found to cause a periodic mode of propagation.³⁹

Experiments performed aboard the KC-135 were inconclusive with benzyl acrylate (a thermoplastic) because of the short time period in weightlessness and the lack of pressure control in the reactor. Interesting results were obtained with triethylene glycol dimethacrylate (a thermoset) in which bubbles were produced by the peroxide initiator.⁵⁴⁻⁵⁶ In high g, they found that long chains of bubbles would form and proposed that existing bubbles would act as nucleation sites for further bubble formation. In low g, the bubbles would move toward the center of the test tube through surface-tension induced-convection bringing the bubbles into closer contact where they could coalesce and grow. The pressure was not controlled during the reaction, and the velocity could not be independently varied from the amount of gas evolved because the initiator controlled the velocity and produced the gas. Therefore, we undertook a study in which a blowing agent was added to systems using a gas-free initiator and in reactors with a piston that allowed isobaric conditions.

The addition of an aqueous blowing agent to the reaction mixture results in the boiling of the blowing agent at the front. At the front, a viscosity gradient exists where the change from low conversion to higher conversion provides a soft "gel region" in which bubbles can nucleate and grow until the front passes, and the polymer becomes rigid. Bubble size can be controlled by varying the amount of blowing agent added, and the boiling temperature of the blowing agent. Bubble distribution can be controlled by varying the concentration of surfactant in the blowing agent mixture.

Bubbles are formed at the front where there is a sharp concentration gradient. The polymer in this region is soft and the bubbles can expand until the front passes, and the polymer gels and traps the bubbles. Figure 12 shows a frontal polymerization reaction in which bubbles are formed near the front and trapped in the polymer

In order to investigate the effects of gravity on the properties of foams produced via frontal polymerization, experiments were performed aboard the NASA KC-135 aircraft. Using frontal polymerization for reduced gravity studies offers both advantages and disadvantages compared to the previous reduced gravity experiments.^{49, 50, 52} With multifunctional acrylates, the polymer gels rapidly so that the cells formed are not affected by the changes in gravity produced by the KC-135. This also allows us to view the effects of different levels of acceleration on the foam produced because the front propagates through several parabolas, which provides an internal standard for comparison of the effects of various levels of gravity. Another advantage is the simplicity -- no chemicals need to be mixed during flight.

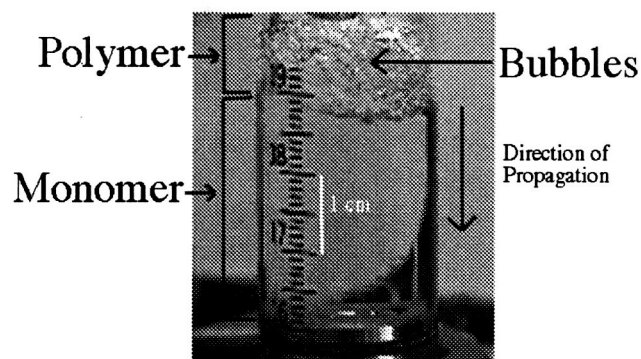


Figure 12. A foaming system consisting of a monomer mixture containing HDDA, HEMA, Aliquat Persulfate, Aliquat 336, and Water. The piston on the bottom allowed the reaction to occur at constant pressure.

The main disadvantage is that the bubbles produced in the microgravity region of the parabola tend to coalesce and grow larger in an attempt to minimize their surface free energy. The bubbles become larger than the gel region of the front, and they are essentially pushed ahead of the front until the high g pullout. Another disadvantage is the elongation of the cells formed as they interact with the glass walls of the test tube. This allows for the overlap of the cells produced in one region of the parabola into the next region of the parabola. Also of major concern is the amount of time required to initiate the reaction, and the amount of time required for the front to propagate the length of the test tube. Systems with higher front velocities can be used but since the KC-135 can only produce 20 seconds of reduced gravity, the timing of the initiation of the reaction is very important in the acquisition of useable results.

Of course, for thermoplastics the polymer has a sufficiently low viscosity that during the high g phase, the bubbles rise and the polymer sinks.

Experimental

Liquid/Solid system

The reaction systems consisted of a monomer mixture containing 90% 1,6-hexanedioldiacrylate (HDDA; technical grade; Aldrich), with 10% 2-hydroxyethylmethacrylate (HEMA; Polysciences), which was added to slow the front velocity so that multiple parabolas could be seen in the same sample. A 10% Aliquat persulfate (tricaprylmethyl ammonium persulfate, APS), synthesized according to the procedure of Chekanov et al.⁵⁷ solution was added to the monomer mixture as a bubble-free initiator. This reaction mixture results in a rigid crosslinked polymer that will retain the cellular structure throughout the flight. The blowing agent solution was made up of 5% Aliquat 336 (Aldrich) and 95% distilled water. The Aliquat was added as a surfactant to allow the water to be dispersed in the organic monomer solution. All reagents were used as received.

The apparatus was the same as used on the *Conquest I*.⁵³ The reaction mixture was placed in a test tube, and a piston was inserted to allow for the expansion of the gas without a buildup of pressure inside of the test tube. A heater was attached, and the test tube was placed inside of a

hermetically sealed glass chamber. The apparatus used is shown in Figure 13. When the target parabolas were achieved, the heaters were turned on and the reactions video taped.

Liquid/Liquid System

The reaction system consisted of 91% hexyl acrylate (Aldrich) as the monomer, 5% Aliquat persulfate as the free-radical initiator, and 4% Luperox 231 (1,1-di(t-butylperoxy)-3,3,5-trimethylcyclohexane; Atochem) as both an initiator and blowing agent because it decomposes to form free radicals and volatile products (methane and acetone).

The apparatus was built by the Marshall Space Flight Center (MSFC). It provided three levels of containment for two samples per flight, rapid ignition of the fronts and video. A three-axis accelerometer measured acceleration levels to 0.001 g, and the values can be seen in the images. A negative value indicates "normal" acceleration downward. For example, during the high g pull-out-, the middle accelerometer (2) would read - 1.6 g.

Viscous Liquid/Liquid System

The reaction system was made more viscous by adding poly(hexyl acrylate) to the mixture. The poly(hexyl acrylate) was prepared by bulk polymerizing a 1% Luperox 231/ 99% hexyl acrylate solution in an oil bath at 110 C for 30 minutes. The reaction mixture consisted of 20% of the polymer, 5% Aliquat persulfate, 2% Luperox 231, and 73% hexyl acrylate.

Apparatus

The apparatus was built by the FPM team at NASA MSFC. Diagrams of the apparatus used for the KC-135 flights are shown in Figure 13 below. The test tube containing the initial reactants and a piston to allow for the expansion of the gas was inserted into the glass containment chamber and a cartridge heater was attached. Illumination of the reaction was provided by a flat panel light positioned behind the chamber and the reactions were monitored with video cameras mounted on adjustable positioning tracks. The apparatus was contained inside of an outer casing that provided a third level of containment and protected the internal components of the reactor. The entire apparatus is attached to the structural support and connected to the power supply and video control rack. Video images were recorded using digital VCR's on the rack.

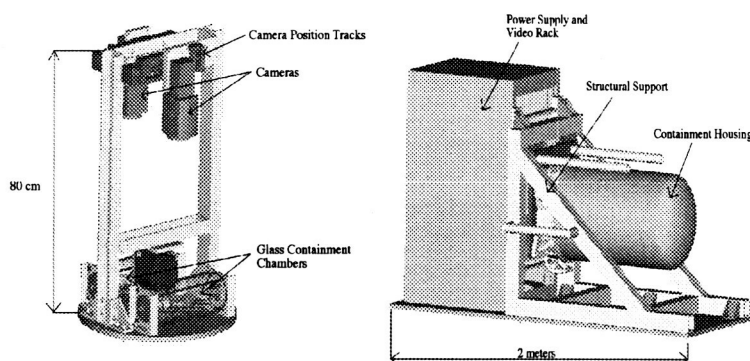


Figure 13. Diagrams of the apparatus used aboard the KC-135 aircraft for the liquid/liquid experiments. Courtesy of Steve Fischer.

Discussion

Liquid/Solid System

In laboratory-based experiments, we found that the size and distribution of the bubbles were nearly uniform (Figure 12). The bubble size increased as g decreased, but there was an overlap of the bubbles produced in microgravity into the region produced in high g as seen in the diagram in Figure 14. This overlap of phases of g -level eliminated our ability to measure the density of the foams produced, but the dramatic differences bubble size in each level leads us to believe that there would be a significant change in the density of the foam regions formed in microgravity compared to those regions formed in high g if samples were formed exclusively in low g . Because the systems propagated so slowly, this was not possible to achieve. A pure HDDA system would propagate rapidly enough but it was impossible to time the start of the front to overlap with the low g period.

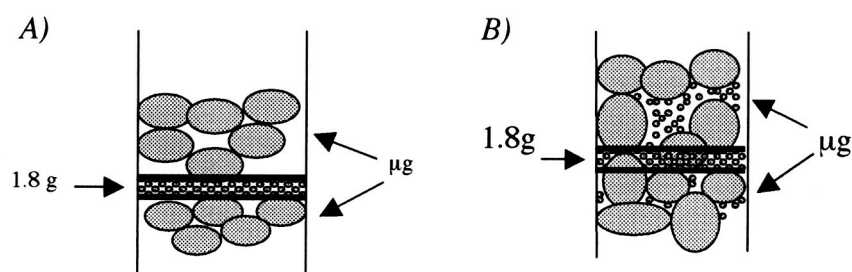


Figure 14. Schematics of expected (A) and observed (B) bubble size distribution.

Inspection of the video tapes and the samples from the flights also revealed one other interesting result. We found that in microgravity, the large bubbles were coalesced ahead of the front, but were surrounded by series of small cells when the high gravity phase was achieved. This can be seen in the images in Figure 15.

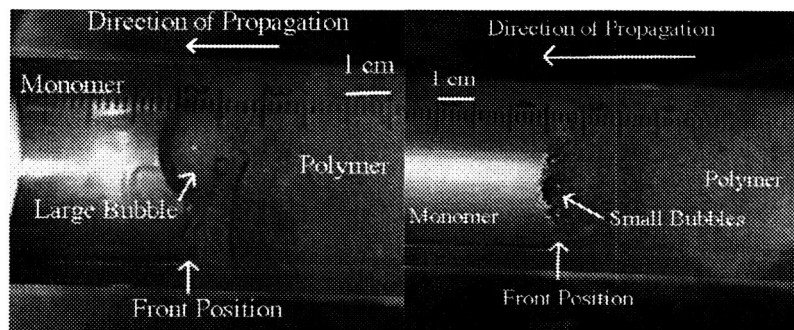


Figure 15. Images of foams produced in Low gravity (left) and High gravity (right). The systems consisted of HDDA, HEMA, Aliquat Persulfate, Aliquat 336, and water. The 1.8 g and μ g images were taken from the same sample at different times during the flights.

Liquid/Liquid Systems

The use of a monofunctional acrylate provides a thermoplastic system that has the potential for use as an insulation and/or a cushioning foam. Since there is no crosslinking, the polymer does not become rigid but becomes viscous as it cools. In a system of this sort, the bubbles produced at the front are carried up by buoyancy. In weightlessness, there is no buoyancy, so the bubbles formed remain stationary, which allows the polymer to cool and increase in its viscosity while the bubbles are not moving. We found that aboard the KC-135, g-jitter causes the bubbles to move constantly. (Variations as large as 0.1 g were observed.) Several other dynamical variables also played a role in the problems observed. Thermocapillary migration of the bubbles toward the center of the test tube allowed many of the bubbles to coalesce to form very large bubbles in the front.

Bubble nucleation occurs at the front as the Luperox is decomposed. The bubbles begin slowly migrating upwards while they still continue to expand. The larger the bubble gets, the faster is the migration rate. Because of the piston, a void forms above the front. Another complication is that because of the high g period, the Rayleigh-Taylor instability caused polymer to sink, increasing the viscosity at the bottom of the tube.

We also observed migration of the bubbles toward the center of the tube as they rise. There are two possible mechanisms for this migration. The central axis of the test tube has a significantly higher temperature than at the walls. This causes thermocapillary migration of the bubbles toward the hotter region.⁵⁸ The second possible reason for the lateral migration is that convection behind the front causes the bubbles to be pushed by the convective current into the center. We have seen instances when a current can be seen to push the bubbles behind the front. On several occasions, we have observed bubbles near the walls being pushed downward as they grow, and when the size of the bubble becomes large enough, buoyancy carries the bubbles upward. In reduced gravity, the convection stops, and we observe the thermocapillary migration of the bubbles toward the center of the test tube where the temperature is the highest. Images taken from the KC-135 videos can be seen in Figure 16.

When the bubbles migrate toward the center, three phenomena occur. First, the bubbles become spherical because there is no buoyancy. The second is that fewer small bubbles are formed because the bubbles are essentially at rest, and most of the evolved gasses will feed into pre-existing bubbles. The third phenomenon is that as the bubbles grow larger, they begin to pinch off. (A drop can only be stretched to p times its diameter before it breaks.⁵⁹) This offers a validation of the results obtained on the *Conquest I* sounding rocket.⁵³

Increasing the Luperox concentration increased the size and number of bubbles but did not alter the qualitative behavior. Using more Aliquat persulfate increased the front velocity but did not affect the qualitative behavior.

We propose that longer periods of reduced gravity would produce a periodic bubble structure in the polymer as can be seen in Figure 17 but which was quickly destroyed by the high g pull out. However, we hasten to point out that large variations in the acceleration level moved the bubbles up and down the tube so that it is impossible to offer a definitive interpretation; longer periods of higher quality weightlessness would be required to test our proposed mechanism.

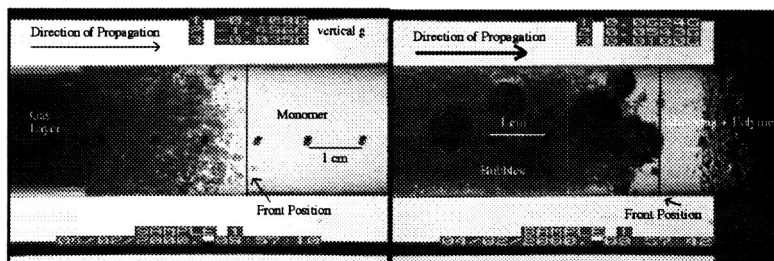


Figure 16. Bubble behavior in liquid/liquid system under (left) high gravity and (right) low gravity.

Viscous Liquid/Liquid System

One way to minimize the effects of g-jitter is to increase the monomer viscosity. We did this by dissolving poly(hexyl acrylate) in the hexyl acrylate. This increased the viscosity of the monomer sufficiently to damp the effects of g-jitter. It also lowered the front temperature. Lowering the front temperature prevents the formation of extraneous bubbles due to dissolved gases and solvents.

As the front nears a region of monomer, the temperature begins to increase rapidly, which rapidly decreases the viscosity. This allows for a smaller region of convection where we can observe bubble migration near the front. When the front reaches that region, the viscosity begins to increase as the monomer is converted to polymer. The bubbles are still able to move in this region but as the front passes, the temperature begins to decrease causing a further increase in the viscosity of the polymer. The viscosity gradient provides a means for some very interesting dynamic properties of both propagating fronts and bubble interaction.

From the KC-135 experiments, we did see the thermocapillary migration of the bubbles to the center of the test tube and since the viscosity of the mixture was much higher, convective migration is limited to the immediate region around the front. Bubble coalescence also slowed. From this we observed that the bubbles formed in reduced gravity would grow until the regions surrounding those bubbles were devoid of gases. As can be seen in Figure 18, the large bubble produced in low gravity remains approximately centered in the tube. When high gravity is again achieved, buoyancy forces the large bubble up through the polymer and into the gas layer.

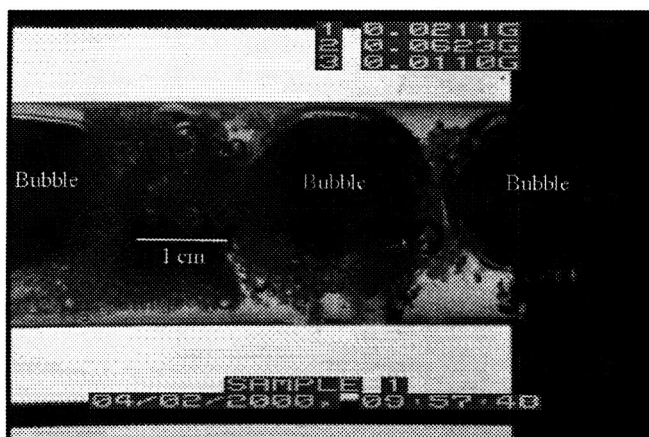


Figure 17. The formation of a transient periodic bubble structure in the liquid/liquid system

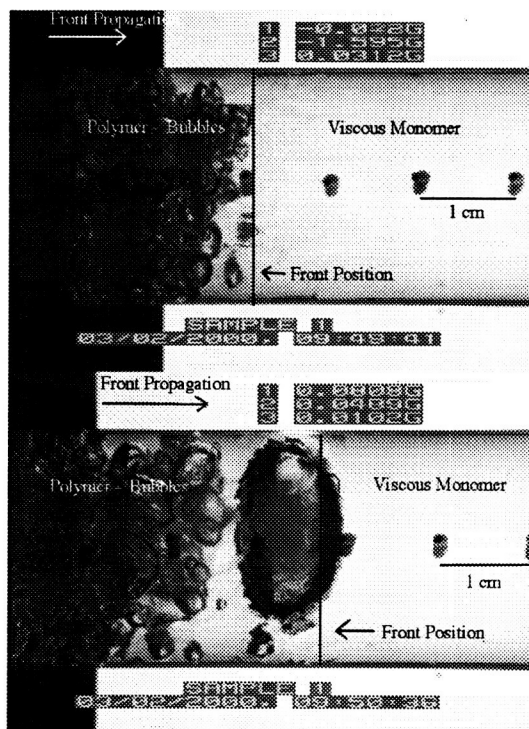


Figure 18. Viscous liquid/liquid system in high (1.6) g (top) and low(0.05) g (bottom)

Conclusions

Frontal polymerization may provide a viable method for producing foams in space. These KC-135 flights clearly indicate that the acceleration level significantly affects the bubble behavior in a front. The results support the hypothesis that the periodic structure observed on the *Conquest I* sounding rocket was the result of post-front growth and aggregation and not a periodic phenomenon in the front itself.

Transition to TIPMPS

In August 2000 we realized that goals 2, 3 and 5 of our proposal had been addressed through KC-135 flights. Question 6 was answered in ground-based research, viz, the rapid reaction in frontal polymerization to form thermosets significantly reduces the hydrodynamic effects during phase separation.

The highest priority question was number 1. We supposed that even with miscible polymer/monomer systems an effective interfacial tension existed and that gradients in this tension would be caused by heat loss. The gradients would cause a flow that could interact with the front. However, after performing experiments and analysis, we concluded that three factors affected the effective interfacial tension: temperature conversion and the width of the reaction zone. Observing convection in a front in microgravity would not allow us to evaluate the contributions of each and adequately test the theoretical predictions based on the hypothesis of an effective interfacial tension derived from the Ginzburg-Landau free energy functional. We

requested and were granted a name change for the project. We passed the Science Concept Review on December

Overview: Transient Interfacial Phenomena in Miscible Polymer Systems (TIPMPS)

Almost one hundred years ago Korteweg published a theory of how stresses could be induced in miscible fluids by concentration gradients, causing phenomena that would appear to be the same as with immiscible fluids. Miscible fluids could manifest a “transient” or “effective” interfacial tension (EIT). To this day, there has been no definitive experiment to confirm Korteweg’s model but numerous fascinating and suggestive experiments have been reported.

The goal of this investigation is to answer the question: **Can concentration and temperature gradients in miscible fluids induce stresses that cause convection?** It is impossible to answer the question under 1 g conditions because the same gradients that cause the stresses also cause buoyant forces that overwhelm the Korteweg stresses.

In 1954 Cahn and Hilliard published their landmark thermodynamic analysis of diffuse interfaces in immiscible materials based on square gradient theory. Although they used different approaches, their mathematical results are similar to Korteweg’s. Both approaches have a single parameter, k and involve the square of the concentration gradients. We use the Cahn-Hilliard theory to extract the value of k for a monomer and its miscible polymer from spinning drop tensiometer experiments. Using this parameter in the Korteweg stress model with the Navier-Stokes equations, we predict transient, measurable fluid flows caused by externally-imposed gradients along a miscible interface between a monomer and its polymer. This experiment will constitute a definitive test of Korteweg’s theory.

An interface between two miscible fluids can best be created via a spatially-selective photopolymerization, which allows the creation of precise and accurate concentration gradients between polymer and monomer. Optical techniques will be used to measure the refractive index variation caused by the resultant temperature and concentration fields. The convection induced by variations in the interfacial width can be studied independently from that caused by temperature and concentration gradients with a uniform interface width. Thus, the applicability of the square gradient energy term with a constant gradient energy parameter far from equilibrium can be tested and the relationship between the EIT measured by spinning drop tensiometry and Korteweg stresses confirmed.

Because the large concentration and temperature gradients cause buoyancy-driven convection that prevents the observation of the predicted flows, the experiment must be done in microgravity.

The results will not only put to rest a one hundred-year-old scientific mystery, they will provide important information on the application of the Cahn-Hilliard theory to miscible fluids. Confirmation of the numerical results will be of interest to all who use phase-field models or Cahn-Hilliard fluid models in simulating immiscible fluids. Knowledge gained from these experiments will permit evaluation of the role that concentration-gradient and temperature-gradient induced convection can play in industrial processing of miscible polymer systems. Finally, demonstrating that convection can occur in microgravity in miscible systems will be important to space processing of materials.

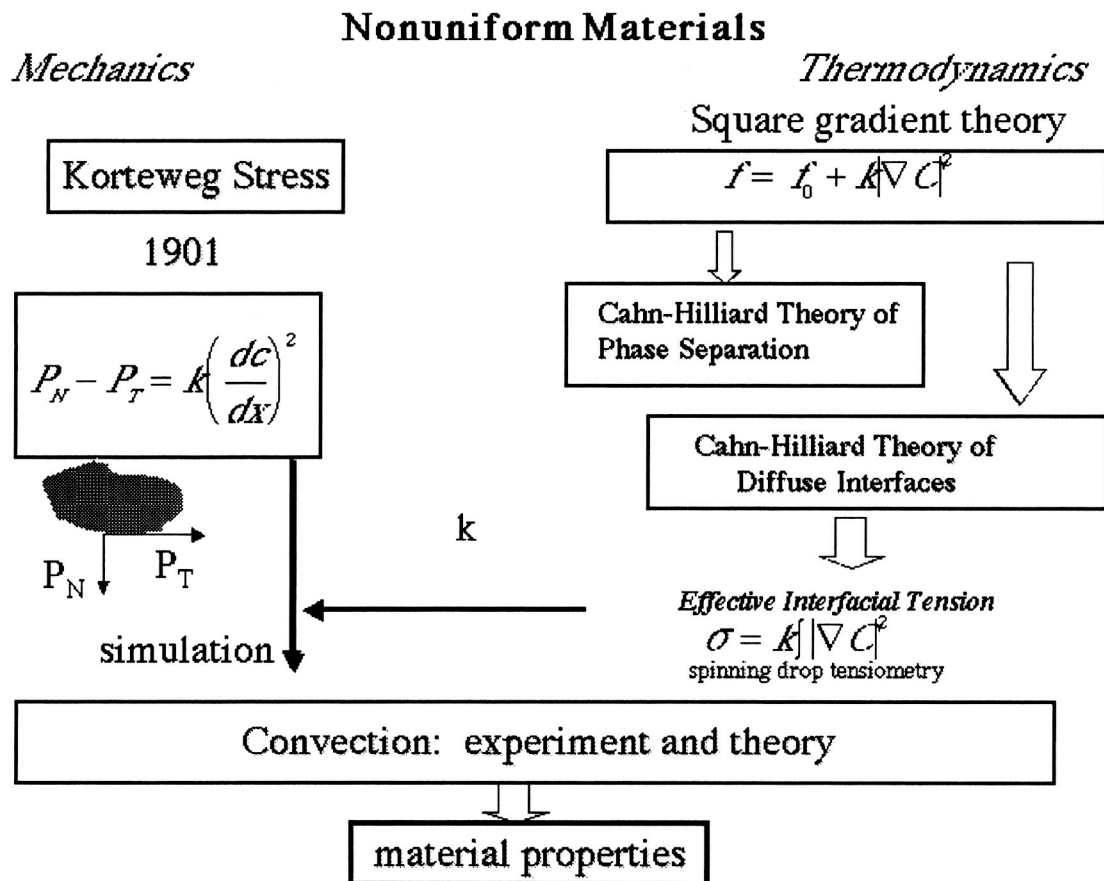


Figure 19. Overview of Project.

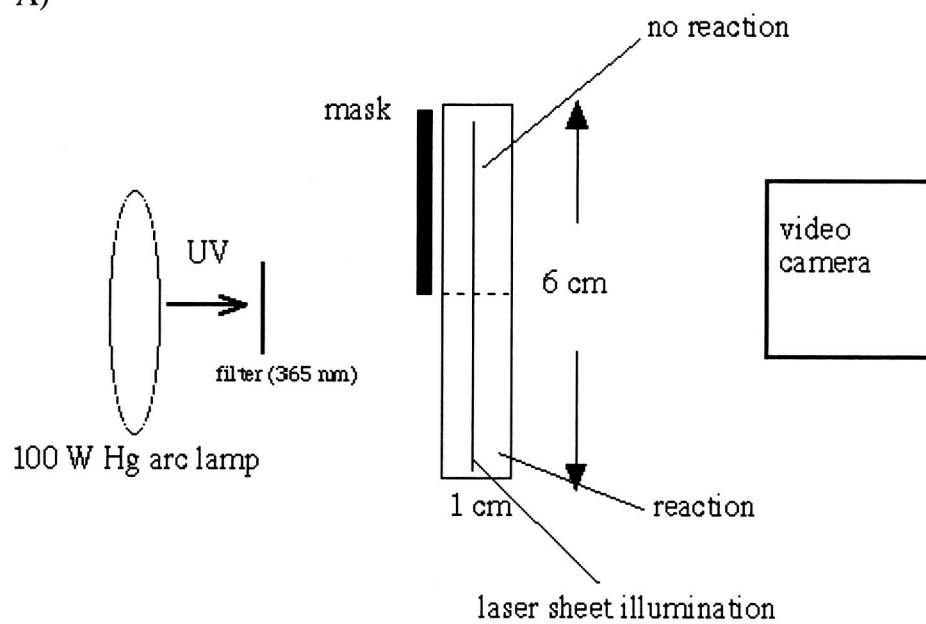
Description of Experiments

A sharp transition zone between poly(dodecyl acrylate) and dodecyl acrylate, which are miscible, will be created by photopolymerizing dodecyl acrylate in a rectangular cuvette 3 x 6 x 1 cm. We illuminate the reactor with 365 nm UV light using masks that create a known interfacial profile between monomer and polymer in 10 seconds. In some experiments a temperature gradient will be applied

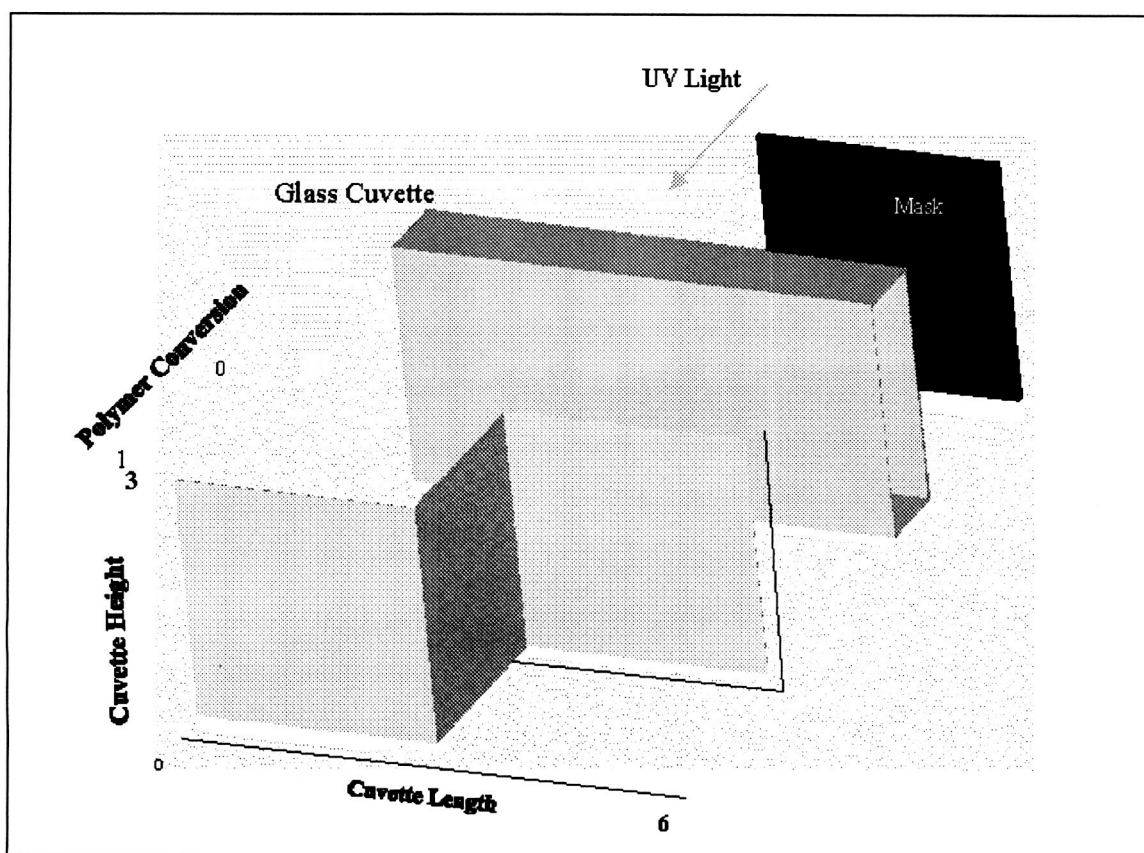
The viscosity will be measured using the shift in fluorescence of pyrene. The fluid flow will be measured by Particle Imaging Velocimetry (PIV) for ten minutes. The temperature field and the refractive index field will be measured for ten minutes, allowing the calculation of the concentration field.

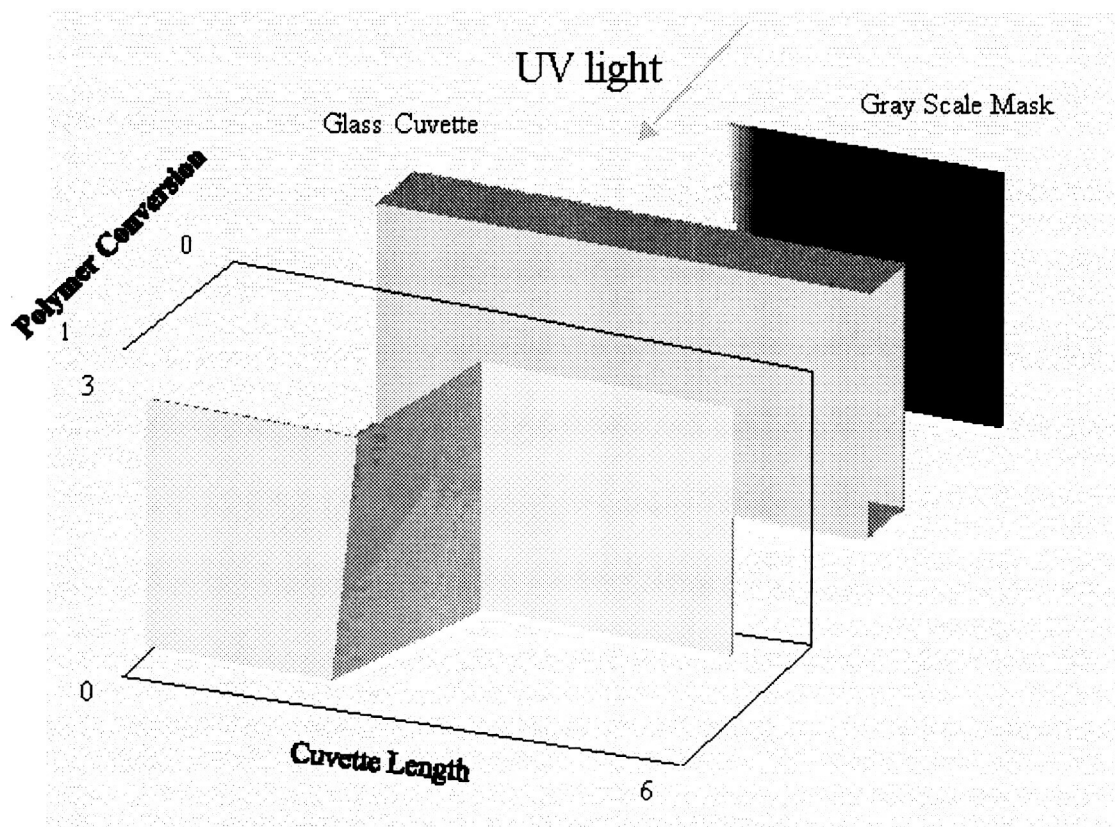
Figure 20 shows schematic representations of the experimental set-up and how the mask produces two regions -- one of unreacted monomer and one of hot polymer. The transition zone can be controlled by the type of mask that is employed.

A)



B)





C) **Mask Types.** Each mask consists of three regions.

Mask 1

Mask 3



Figure 20.

The samples will consist of three regions. The first region is the monomer region, the second region is the transition zone between the monomer and polymer regions, and the third region is the polymer region. The samples in Experiments 1 and 3 will be produced by using a mask that produces a sharp transition zone between the monomer (3 x 3 cm) and polymer (3 x 3 cm) regions. For Experiment 2, several different masks will be employed that have different transition zones between the area of no transmittance and complete transmittance.

Scientific Knowledge to Be Gained

We will test Korteweg's prediction that concentration and temperature gradients can cause stresses in miscible fluids by creating known stresses and measuring the convection that results.

We will verify that the Cahn-Hilliard theory for the interfacial tension can be applied to miscible fluids.

Value of Knowledge to Scientific Field

There have been numerous reports of effects in miscible fluids that have been explained in terms of a transient, or effective, interfacial tension caused by sharp but transient concentration gradients. For example, Maxworthy is studying the displacement of a fluid by another miscible fluid, and the EIT between the fluids is believed to be important.⁶⁰ However, to our knowledge, no one has studied if convection could be caused by gradients in this EIT. Our work predicts that convection analogous to surface-tension induced convection (STIC) can occur at the transient interface of two miscible fluids, a phenomenon we refer to as "Effective Interfacial Tension Induced Convection (EITIC)." Verification of our predictions for fluid flow will be an exciting and novel finding.

Secondly, demonstrating the existence of this phenomenon in miscible fluids will open up a new area of study for materials science. Many polymer processes involving miscible monomer and polymer systems could be affected by fluid flow and so this work could help understand miscible polymer processing, not only in microgravity, but also on earth.

The Cahn-Hilliard theory of diffuse interfaces is also based on the square gradient term of the free energy and yet the significance to miscible fluids is not clear. Our experiment directly tests the applicability of the square gradient energy to miscible systems. Not only does it relate to polymer processing but also the understanding of all phenomena analyzed in terms of a square gradient theory.

The modeling techniques we use can be applicable to a wide array of problems with and without interfaces.

Justification of the Need for Space Environment

The concentration and temperature gradients necessary for EITIC also produce buoyancy-driven convection. Increasing the viscosity would eliminate the effect of buoyancy but only at the price of suppressing the flows we seek to study. Thus, we need to make the Rayleigh number (or Grashof number) zero or nearly zero without increasing the viscosity. This can only be accomplished by reducing the effective value of g to microgravity levels.

As expected, ground-based experiments were overwhelmed by buoyancy-driven convection. Our calculations indicate that the g level must be reduced to at least 10^{-5} g in order to reduce the buoyancy-induced flow to a level that will not interfere with the observation of EITIC. To create the polymer/monomer interface requires at least 10 seconds. Moreover, in order to test the long-term behavior of the EITIC, experiments must run for at least 5 minutes, much longer than the time afforded by drop towers.

Background

Free Energy of Nonuniform Fluids

A single fluid at equilibrium has a free energy that is constant throughout the volume. The free energy of a nonuniform fluid can be treated by including a term proportional to the square of the concentration gradient. The expression for the free energy at a location is now a functional because it depends on the concentration beyond the location. Cahn and Hilliard developed the theory based on what is often called the Ginzburg-Landau free energy functional, in 1958.⁶¹ We briefly summarize their results:

Consider a medium in a volume Ω . Its Helmholtz free energy can be represented as

$$F = \int_{\Omega} f(x) dx \quad (3)$$

where $f(x)$ is a free energy density,

$$f = e - Ts, \quad (4)$$

e is the specific internal energy, s the entropy and T is the temperature.

Suppose that the medium consists of two different liquids with densities and denote $c(x)$ as the mole fraction of the first liquid. If we take into account nonlocal interactions of molecules in the liquid, the internal energy can be written as

$$e(T, c) = e_0(T, c) + k|\nabla c|^2 \quad (5)$$

where ∇c is the composition gradient. Therefore, we have

$$f = f_0 + k|\nabla c|^2 \quad (6)$$

where

$$f_0 = e_0 - Ts. \quad (7)$$

The free energy functional takes the form

$$F = \int_{\Omega} f_0 + k|\nabla c|^2 dx \quad (8)$$

The free energy, f_0 , as a function of composition can have one or two minima.

We first consider the case with a single minimum. The minimum of the free energy is reached on a distribution $c_0(x)$, which satisfies the equation

$$k\Delta c - f_0'(c) = 0 \quad (9)$$

In the neighborhood of the minimum c_0 , $f_0'(c)$ can be approximated by a linear function,

$$f_0'(c) = a(c - c_0). \quad (10)$$

It is important to note that $a = f_0''(c_0)$ is positive. Hence, the only solution of the equation

$$k\Delta c - a(c - c_0) = 0 \quad (11)$$

is the uniform distribution $c \equiv c_0$. This means that the two liquids are miscible.

It remains the same for the double-well potential near the points $c_0^{(1)}$ and $c_0^{(3)}$. In the neighborhood of $c_0^{(2)}$, $a = f_0''(c_0)$ is negative, and equation (9) can have a nonuniform solution. The free energy reaches its minimum on this nonuniform solution, and phase separation occurs. Thus the liquids are miscible if their average composition, c , satisfies the condition $f_0''(c_0) > 0$.

The arguments above describe behavior of the system close to equilibrium, in the case of spinodal decomposition, or at equilibrium, for diffuse interfaces. For systems far from equilibrium, the composition can be nonuniform even if the liquids are miscible.

We can write the free energy functional as

$$F = \int_{\Omega} f_0 dx + \sigma A \quad (12)$$

where

$$\sigma = k \int_{\Omega} |\nabla c|^2 d\xi \quad (13)$$

is the effective interfacial tension, and A the area of the interface. The integral in (13) is taken across the interface.

Hence we see that the free energy increases with an increase of the interface area. Since a system tends to minimize its free energy, we need to do work to increase A . The work is proportional to the effective interfacial tension.

If we consider a linear concentration gradient in one dimension, we can write:

$$\sigma = k \frac{\Delta c^2}{\delta}, \quad (14)$$

where δ is the length over which the concentration changes, and Δc is the difference in composition (Figure 21). Of course, this only applies if δ is not too small.

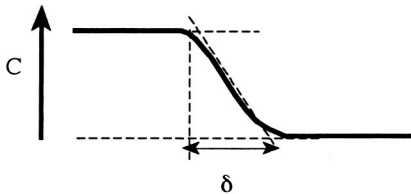


Figure 21. A schematic of an interface between miscible fluids.

Cahn and Hilliard applied this analysis to systems with two coexisting phases at equilibrium but when the interface would be diffuse, such as near the critical point.⁶¹ Whether this also applies to a system arbitrarily far from equilibrium is not obvious.

Rousar and Nauman demonstrated that assuming a linear concentration gradient the surface tension can be found without assuming the system is at equilibrium.⁶² They demonstrated analytically that across a linear concentration gradient, there is a difference between the pressure normal to the "interface" and pressure tangential to it:

$$p_N - p_T = k \left(\frac{dc}{dx} \right)^2 \quad (15)$$

Notice that this is an expression for the Korteweg stress.⁶³

If we integrate across the interface we calculate

$$\sigma = \int k \left(\frac{dc}{dx} \right)^2 dx \quad (16)$$

Theory of diffuse interfaces

Anderson et al. reviewed diffuse interface methods in fluid mechanics.⁶⁴ Basically, instead of treating the interface as a infinitely thin, the explicit variation in density at the interface is accounted for, as van der Waals first did in 1893.⁶⁵ Others have built on this work.⁶⁶

The case of the liquid/vapor interface is not of direct interest to us. However, there are many examples in which the interface between fluids is diffuse and modeled as such using what are often called "phase field models". Antonoviskii⁶⁷ treated the problem using such a model and examined thermocapillary flow (STIC).

Jacqumin modeled contact-line dynamics.⁶⁸ He also modeled two-phase Navier-Stokes flows using phase-field modeling.⁶⁹ He was able to model the Rayleigh-Taylor instability with the

Navier-Stokes equation with an additional forcing term proportional to the square of the concentration gradient. He demonstrated that the traditional sharp-interface Navier-Stokes equations are recovered as the interface thickness and the diffusivity go to zero.⁶⁹

Jasnow and Vials modeled "thermo-capillary" flows (STIC) using a similar approach to Jacqmin, which they called a "coarse-grained description".⁷⁰ With a temperature dependent square gradient energy parameter, they could simulate the migration of an immiscible drop in a temperature gradient and spinodal decomposition of a binary fluid in a temperature gradient.

Korteweg Stresses

Korteweg proposed in 1901 that a nonuniform concentration distribution leads to stresses in a fluid.⁶³ Anderson and McFadden modeled internal waves in a near-critical fluid using a Korteweg stress term in the momentum equation.⁷¹ Joseph and Renardy considered many aspects of Korteweg stresses in miscible fluids.⁷²

How do we relate the Korteweg stress to effective interfacial tension? Equation (14) is also the relation for the Korteweg stress if the fluid is miscible. When we integrate across the interface, we recover the effective interfacial tension (eq. 14). We note that the concept of an interfacial tension is the mechanical analog of the Korteweg stress in the limit of an infinitely-narrow interface (N m^{-1}). We use the thermodynamic formulation when we refer to the interfacial energy (J m^{-2}).

Experimental Evidence for an Effective Interfacial Tension in Miscible Fluids

We now proceed to the experimental evidence for an effective, or transient, interfacial tension between miscible fluids. Joseph and Renardy have impressive pictures of behavior in miscible fluids that appears to follow behavior attributed to interfacial tension.⁷²

Consider the following experiment: An immiscible system exists with two fluid layers. The temperature is rapidly raised above its Upper Critical Solution Temperature (UCST), the critical value such that the fluids are now miscible. What happens? An interfacial tension will exist between the fluids, which will relax toward equilibrium as the concentration gradient at the interface relaxes through diffusion. Thus an *effective interfacial tension* (EIT) can exist between miscible fluids.

May and Maher performed this experiment using a solution of butyric acid and water (62.1 %), which has an upper critical solution temperature at 26.310 C.⁷³ They rapidly raised the system's temperature above its UCST. Using the relaxation rate of thermally excited capillary waves determined by light scattering from the interface, May and Maher were able to demonstrate that the interfacial tension exists between the miscible phases but decreases with time through diffusion.

Others have reported phenomena with miscible fluids that have been explained in terms of an effective interfacial tension. Garik et al. injected water into a CuSO_4 solution or glycerin into water. They proposed that the pattern formation they observed was not viscous fingering but an interfacial-tension induced instability.⁷⁴ Ma et al. performed a theoretical work including molecular dynamics simulations of initially miscible fluids showing that the effective interfacial tension relaxes according to a $1/t^{1/2}$ rule.⁷⁵ Mungall reported that miscible molten silicates form a meniscus, indicating an interfacial tension.⁷⁶ He proposed a theoretical model in terms of the gradient stresses. Castellanos and Gonzalez proposed that the wave length selection in the

electrohydrodynamic instability between miscible fluids of different conductivities can be explained by a transient interfacial tension.⁷⁷

Petitjeans and Maxworthy estimated the same quantity from the wavelength selection of the displacement of water into glycerin in a capillary tube and determined a value of 0.43 mN/m.⁶⁰

Spinning Drop Tensiometry

The interfacial tension between two fluids can be measured using spinning drop tensiometry, which was developed by B. Vonnegut.⁷⁸ The principle is simple: The more dense fluid is placed into a capillary that is rotated at $> 5,000$ rpm (Figure 22). A drop of the less dense fluid is injected into the capillary. The drop is subject to a pressure jump across the interface, which stretches the drop along the axis of rotation. If this were the only force, the drop would extend until it reached the ends of the capillary and form a column of fluid inside the more dense phase. Because the volume of the drop is fixed, as the drop stretches, its area increases. Thus the free energy of the surface increases. The longer the drop and the smaller the radius, the lower is the rotational energy but necessarily the surface area is greater. Thus the equilibrium drop radius can be found by finding the minimum energy as a function of radius.

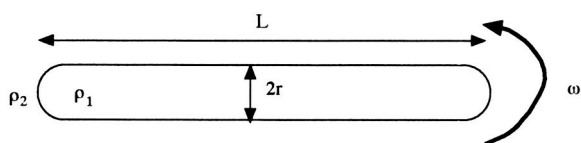


Figure 22. Schematic of a spinning drop

(17-19)

$$E_{\text{surface}} = \sigma(2\pi rL + 4\pi r^2)$$

$$E_{\text{rotation}} = \frac{1}{4}\pi\Delta\rho\omega^2 Lr^4 + \frac{4}{15}\pi\Delta\rho\omega^2 r^5$$

and for $L \gg r$, we have the simple relationship:

$$\sigma = \frac{\Delta\rho\omega^2 r^3}{4} \quad (20)$$

Measuring the Effective Interfacial Tension using Spinning Drop Tensiometry

Using a Krss tensiometer and a custom-built high temperature tensiometer (in the lab of D. Joseph at University of Minnesota), which can measure an interfacial tension with sensitivity of 0.000001mN/m, we studied the effective interfacial tension for two miscible systems. We had two goals:

1) Test the hypothesis that an effective interfacial tension existed between miscible fluids, including dodecyl acrylate and its polymer.

2) Estimate the gradient energy parameter in the free energy functional for dodecyl acrylate/poly(dodecyl acrylate) and determine its temperature dependence.

The capillary was filled with the polymer, whose temperature was controlled within 0.1 °C. The drop was injected and then the capillary rapidly spun up to its operating speed. The drop radius was measured with a image analysis system.

The fact that a drop of water, or monomer inside a polymer liquid, does not stretch to the end of the tube immediately is a strong argument for the existence of an effective interfacial tension. The pressure difference caused by the difference in density and the rotation forces the drop to stretch along the rotational axis. There must be a resisting mechanism and that is the effective interfacial tension. Reducing the diameter of the drop reduces the pressure difference but increases the surface area of the drop. Because of the EIT, the increase in area increases the free energy.

What is the natural relaxation time for an immiscible drop? Hu and Joseph simulated immiscible polymer systems with high viscosity, 1000 poise for the drop and 10 poise for the more dense phase and the same density difference as glycerin and water. The viscosity of glycerin is 12 poise so this system is 100 times more viscous. They calculated the relaxation time as less than 100 seconds.⁷⁹ Heinrich and Wolf measured the relaxation time or rotation-jump experiments for viscous polystyrene systems and measured relaxation times of less than 180 seconds.⁸⁰ Petitjeans measured the EIT for glycerin/water and found that the drop diameter reached a quasi-steady value after 100 seconds.⁸¹

A drop of dodecyl acrylate (with added dye) is shown in Figure 23, 130 seconds after rotation was started. Figure 24 shows the evolution of the apparent interfacial tension at 90, 100 and 100 °C.

Estimation of the Square Gradient Parameter

Recall that the Cahn-Hilliard theory of diffuse interfaces predicts that for a linear gradient the interfacial tension has this form:

$$\sigma = k \frac{\Delta c^2}{\delta} \quad (21)$$

For glycerin/water and polymer/monomer (at 200 °C) the values of EIT are approximately 0.6 mN/m. Δc is the difference in molecule fraction, which is one. So we need an estimate of δ , which we can obtain in two ways. One way is to estimate the diffusion distance,

$$\delta = \sqrt{Dt}. \quad (22)$$

Petitjeans and Maxworthy measured the diffusion coefficient for glycerin/water to be on the order of 10^{-6} cm²/s. Taking the time on the order of 100 s, we obtain of 0.01 cm. This is also consistent with a measurement of the gray scale profile of a captured image of a spinning drop.

For polymer at 200 °C, we estimate the width of the transition zone to be 0.3 mm, which would give $k = 1.8 \times 10^{-7}$ N. We use the smaller value in our simulations to provide a lower estimate of the expected flow.

$$\frac{\partial k}{\partial T} = 1.7 \times 10^{-9} \text{ NK}^{-1}$$

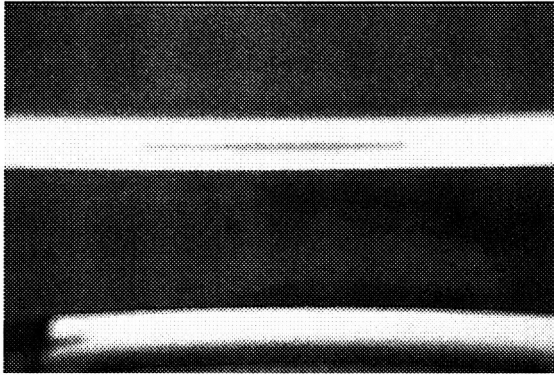


Figure 23. Image of a drop of dodecyl acrylate in poly(dodecyl acrylate) at 100 °C, 130 seconds after rotation was started. $\omega = 3,600$ rpm. Drop length is 6 cm.

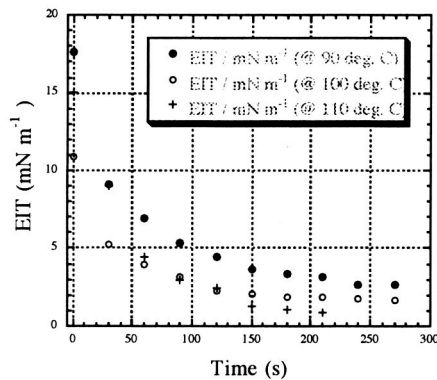


Figure 24. The temporal evolution for the apparent interfacial tension between a drop of dodecyl acrylate in poly(dodecyl acrylate) with a molecular weight of a approximately 80,000.

Modeling of Korteweg Stress: Effective Interfacial Tension-Induced Convection

We developed a mathematical model for Korteweg stresses in miscible fluids in which the stress tensor terms are added to the incompressible Navier-Stokes equation. To study the influence of the effective interfacial tension on a monomer and its miscible polymer we consider mass, energy and momentum conservation. If we assume:

- a) Thermal and diffusive fluxes are small,
- b) The internal energy has the form,

$$e = e_0 + k|\nabla c|^2 \quad (23)$$

- c) capillary forces are tangential to the composition gradient,

d) the fluids are incompressible and have the same density and viscosity, we obtain the following model.

(24-27)

$$\frac{\partial T}{\partial t} + v \nabla T = \kappa \Delta T$$

$$\frac{\partial c}{\partial t} + v \nabla c = D \Delta c$$

$$\frac{\partial v}{\partial t} + (v \nabla) v = -\frac{1}{\rho} \nabla p + \nu \Delta v + \frac{1}{\rho} \left(\frac{\partial K_{11}}{\partial x_1} + \frac{\partial K_{12}}{\partial x_2} \right)$$

$$\text{div } v = 0$$

Where T is the temperature, v is the fluid velocity, p is the pressure, ν is the kinematic viscosity, ρ is the density and c the mole fraction of polymer. K_{ij} are the stress tensor terms, defined by:

(28-30)

$$K_{11} = k \left(\frac{\partial c}{\partial x_2} \right)^2$$

$$K_{12} = K_{21} = -k \frac{\partial c}{\partial x_1} \frac{\partial c}{\partial x_2}$$

$$K_{22} = k \left(\frac{\partial c}{\partial x_1} \right)^2$$

where k is system specific, with units of N.

We emphasize that this k is the same constant in the square gradient energy term, and we have estimated it from the tensiometer measurements.

Assumption (b) follows from the Cahn-Hilliard theory and reflects molecular interactions in fluids that lead to the appearance of forces tangential to the composition gradient (assumption (c)). Finally, we make the last assumption to simplify the model and to separate the influence of various factors that would complicate the interpretation of the results.

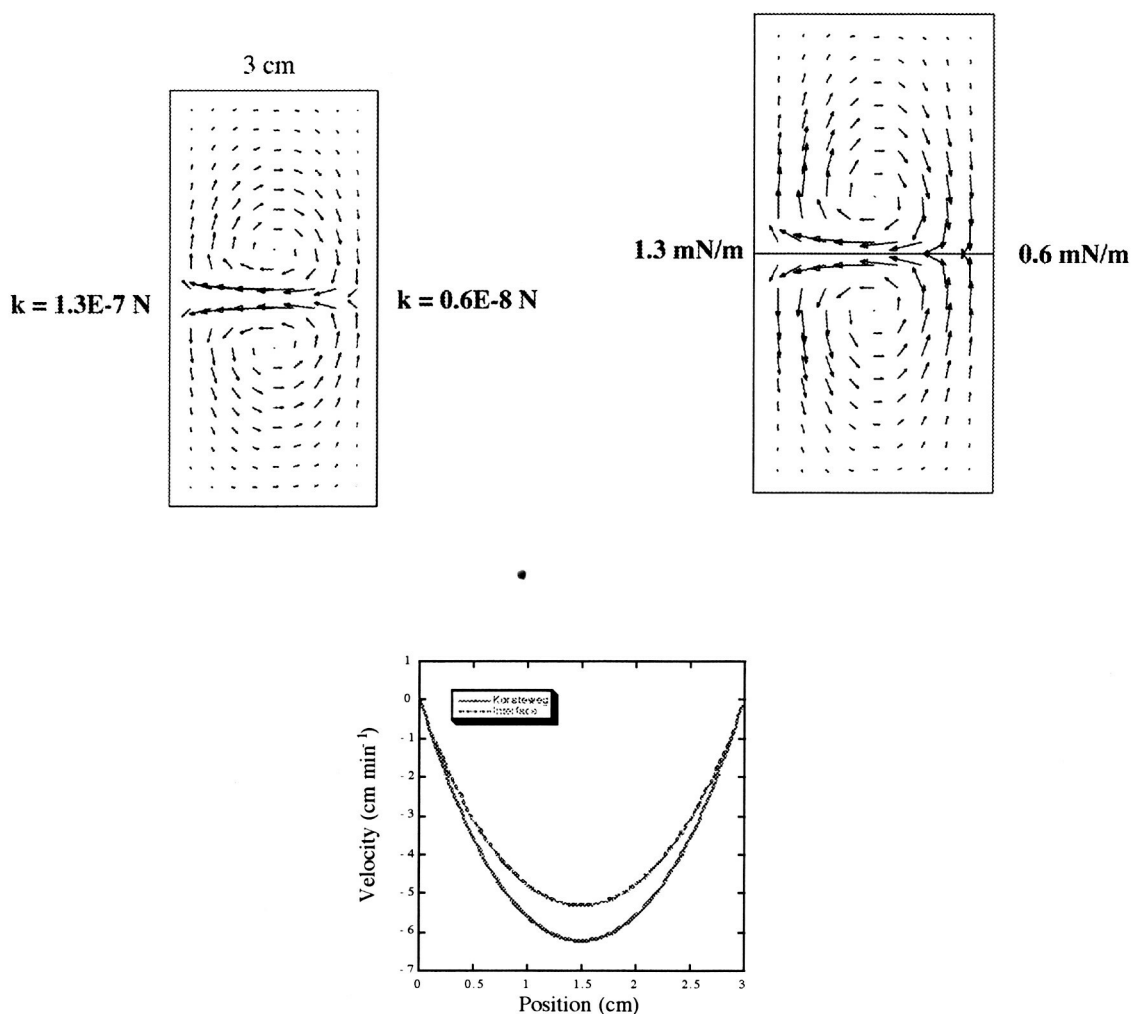


Figure 25. Comparison of diffuse interface to "real" interface simulation for variation in k (left) to gradient in interfacial tension. $\nu = 1 \text{ cm}^2 \text{ s}^{-1}$ Velocity plots: Interface simulation ----, Korteweg —

Validation of Method: Comparison to Interface Problem

Diffuse interface methods, or phase-field modeling, have been shown by several authors to be identical to the classical interface method in the limit of an infinitely narrow interface.^{64, 68, 69, 71} To test the validity of our modeling, we compared the Korteweg calculation for a fixed concentration gradient, which was not perturbed by the flow or diffusion, to a two-fluid interface model. We show now that a width, δ , of 0.01 cm is sufficiently narrow to correspond to the interface model, with the velocity consistently larger than the corresponding interface problem with interfacial tension calculated based on the Cahn-Hilliard formulation for the diffuse interface.

Three sets of simulations were performed:

1) Effect of temperature gradient. Using the Korteweg formulation with $\delta = 0.01$ cm, the k varied linearly to correspond to the effect of a 50 K temperature difference. The interface simulation used the corresponding interfacial tension calculated from the Cahn-Hilliard theory. Figure 25 shows the flow patterns for both simulations and the velocity along the centerline (or interface). Note how similar they are.

2) Effect of concentration gradient. Using the Korteweg formulation with $\delta = 0.01$ cm, the C varied linearly across the "interface" from 1.0 - 0.9. The interface simulation used the corresponding interfacial tension calculated from the Cahn-Hilliard theory (eq. 14).

3) Effect of a variation in transition zone width. In the Korteweg formulation the δ varied linearly from 0.01 cm to 0.1 cm. The interface simulation used the corresponding interfacial tension calculated from the Cahn-Hilliard theory.

Table 1. Temperature Gradient-Induced Convection

	Variation in k , N	Variation in σ , mN m ⁻¹	Maximum velocity
Interface		0.6 to 1.3	5.4 cm min ⁻¹
Korteweg Stress	6×10^{-8} to 1.3×10^{-7}		6.0 cm min ⁻¹

Table 2. Variation in Concentration

	Variation in c	Variation in σ , mN m ⁻¹	Maximum velocity
Interface		0.6 to 0.48	0.9 cm min ⁻¹
Korteweg Stress	$c = 1 - 0.9$		1.0 cm min ⁻¹

Table 3. Variation in Interface width

	Variation in δ	Variation in σ	Maximum velocity
Interface		0.6 mN m ⁻¹ to 0.06 mN m ⁻¹	4.5 cm min ⁻¹
Korteweg Stress	0.01 cm to 0.1 cm		5.4 cm min ⁻¹

In all cases, the Korteweg stress simulations exhibit the same flow pattern and same order of magnitude for the velocity. The interface model has a consistently smaller velocity. Tables 1-3 compare the simulations.

Simulations of the Time-Dependent Flow Field

To determine the relaxation of the flow field we must simulate the time-dependent problem, which is very challenging. The simulations were performed with these parameters:

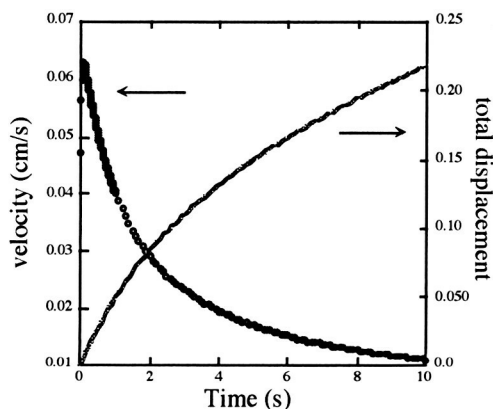
Polymer viscosity = monomer viscosity = $1 \text{ cm}^2 \text{ s}^{-1}$.

Diffusion coefficient, D , = $0.00001 \text{ cm}^2 \text{ s}^{-1}$.

Thermal diffusivity, κ , = $0.001 \text{ cm}^2 \text{ s}^{-1}$. We have performed them with the same viscosity for monomer and polymer, which is temperature independent.

Case 1: Effect of Temperature Gradient

A 50 K temperature difference was imposed over 5 mm along one side, parallel to the transition zone. A flow was created that rapidly relaxed.



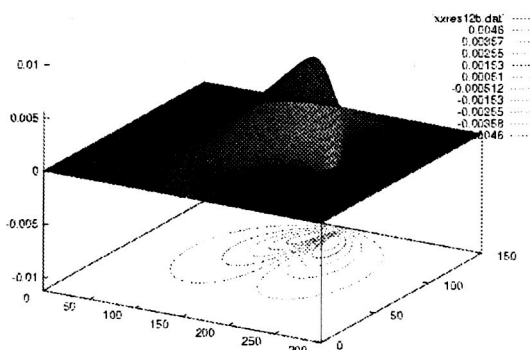


Figure 26. Convection caused a temperature gradient parallel to the interface. A) Streamlines and b) Maximum velocity as a function of time

Case 2: Effect of Concentration Gradient

An isothermal system was simulated in which the concentration, c , along the transition zone varied from 1 to 0.9. A low velocity flow developed.

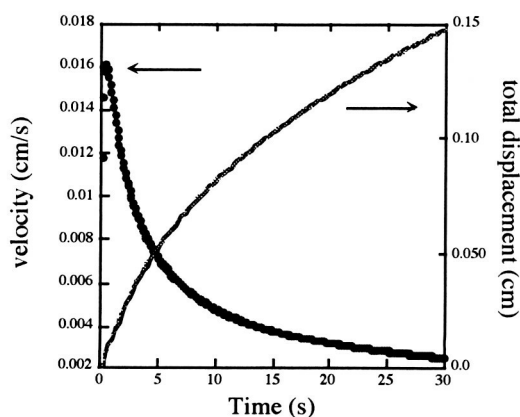


Figure 27. Maximum velocity as a function of time for the convection caused a conversion gradient parallel to the interface.

Case 3: Effect of Interface Width Gradient

The width of the transition zone, δ , was varied from 0.18 cm at one side to 0.9 cm at the other side. Because of numerical difficulties, the more realistically-smaller values could not be simulated so k , the gradient parameter, was increased to compensate. Again, a rapidly relaxing flow was created (Figure 28).

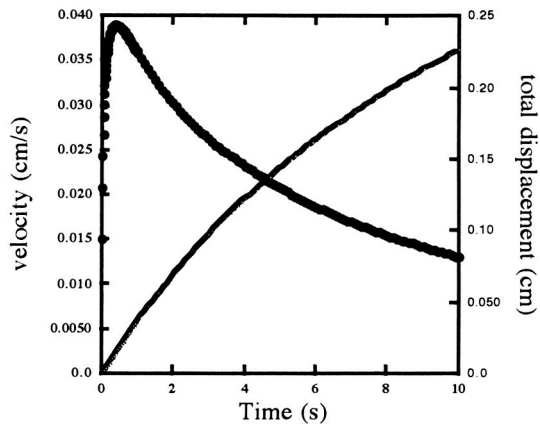


Figure 28. Maximum velocity as a function of time and the total displacement for convection caused a gradient in the interface width.

Observations of glycerin and water in low g

Samples were flown aboard NASA's KC-135 aircraft. The parabolic flights afforded us approximately 20 seconds of low g (about 0.1 g) followed by a minute of 1 - 1.8 g. A glass tube of 2 cm diameter was partially filled with glycerin. During the flight, water was carefully injected on to it. A light bulb (surrounded by aluminum foil) was positioned at the transition zone between the fluids. A rapid temperature gradient could be created (Figure 29).

To minimize the effects of g jitter, the apparatus was free floated during the low g phase of a parabola, being released just after the light was turned on.

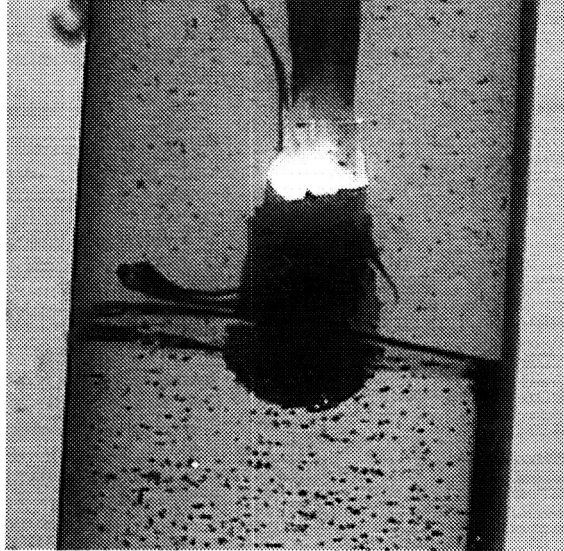
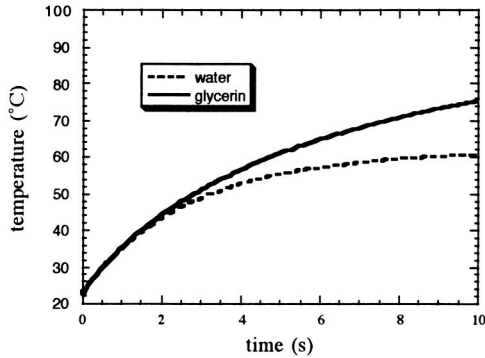


Figure 29. Left: The temperature change caused by the light bulb in water or glycerin. Right: Glycerin under water in a 2.2 cm diameter tube during a free floating experiment.

In Figure 29, we show an image of the glycerin/water during free float. No motion of the particles was observed during the 2 - 3 seconds of free float.

Simulations with temperature and concentration dependent coefficients

We applied another numerical method with the conservation laws (mass, momentum, energy) in integral form (not in differential form) that allows us to introduce a viscosity that is dependent on the concentration.⁸² Instead of the "stream-function and vorticity" we used "pressure-velocity" as the basic variables. We used nonorthogonal Eulerian or Lagrangian meshes.

We first compared the simulation shown in Figure 30 using the more-efficient grid and method but with a constant viscosity. The comparison shown in Figure 30 demonstrates that the two approaches provide the same results.

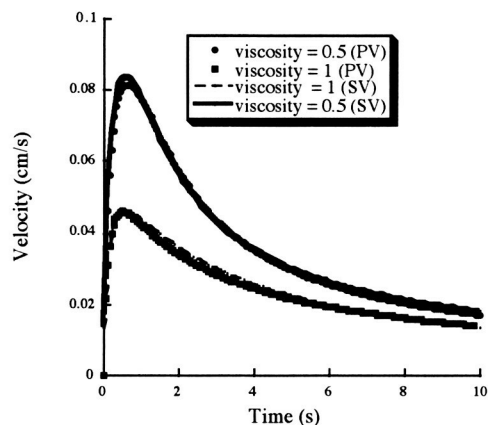


Figure 30. PV indicates the pressure velocity formulation and SV the stream function-vorticity approach for viscosities of 0.5 and 1 $\text{cm}^2 \text{s}^{-1}$.

The function for the viscosity was taken as

$$\nu(c) = \nu_0 e^{\lambda c}$$

shown in Figure 31. Figure 32 shows how the maximum velocity can be higher or lower than in Figure 30. It can be higher because we begin with a viscosity equal to that of the monomer instead of a value equal to that of the polymer.

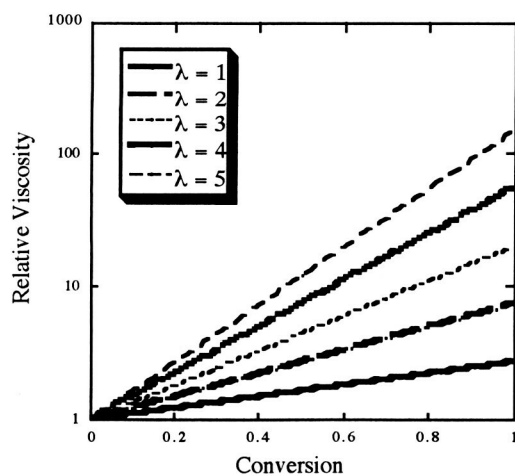


Figure 31. The dependence of the viscosity on conversion for different values of the exponent, λ .

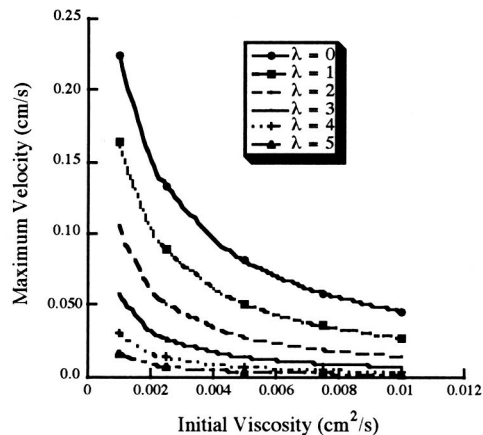


Figure 32. The maximum velocity as a function of the initial viscosity for several values of λ .

Variable Transition Zone with Variable Viscosity

We simulated the fluid flow induced by a variation in the width of the transition zone, δ , from 0.9 mm to 2.7 mm using the variable viscosity (Figure 20).

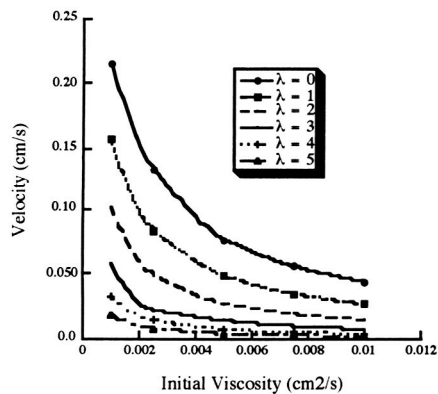


Figure 33. Maximum fluid flow induced by a variation in the width of the transition zone, δ , from 0.9 mm to 2.7 mm

Observations

The maximum flow is strongly dependent on how the viscosity increases with concentration. In all cases, the flow can be significant.

Simulations of Drops and Streams

We spent 2001 preparing a Glovebox experiment, Miscible Drop in Microgravity (MDMG). (Unfortunately, this project was canceled after the ISS cost overruns reduced funding for science.) We simulated a situation close to that of the MDMG experiment in which a drop of water is injected to glycerin or a stream of glycerin is injected into water.⁸³ The simulations are simplified because the viscosity is taken as an intermediate value between that of glycerin and water at 25 °C, $1\text{cm}^2/\text{s}$. For these simulations we used the same code and parameters as for the fixed-viscosity simulations.

For the first case we begin with an elliptic drop (1.2 cm x 0.6 cm) in a domain of 2 cm x 1 cm with a transition zone, δ , of 2 mm.

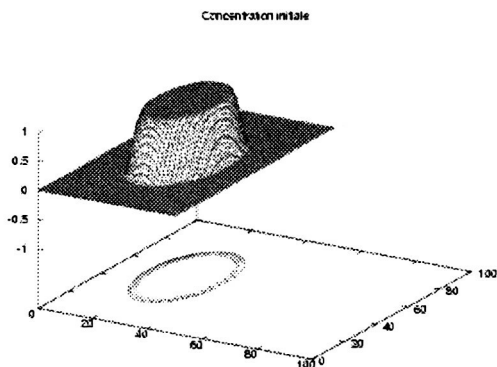


Figure 34. The initial conditions for the drop.

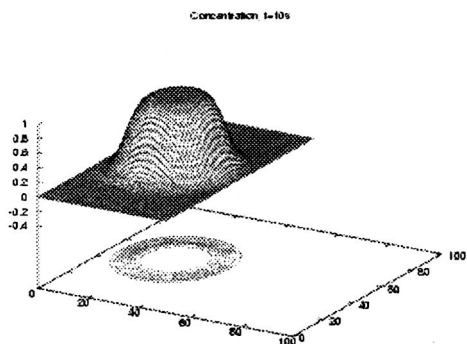


Figure 35. The concentration after 10 sec.

For the long drop the domain is 6 cm x 2cm and the initial dimensions of the drop are: 5 cm x 0.2 cm. The width of the transition zone is 1.2mm.

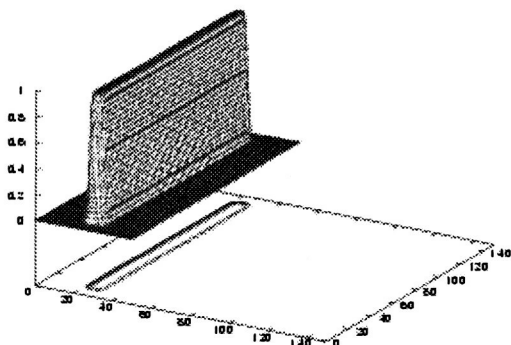
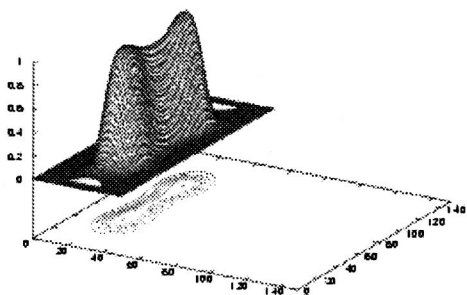
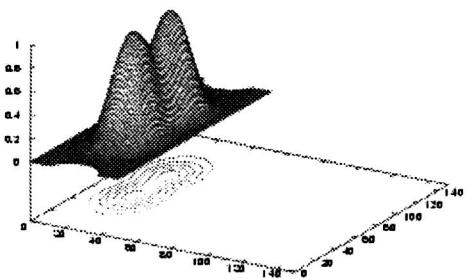


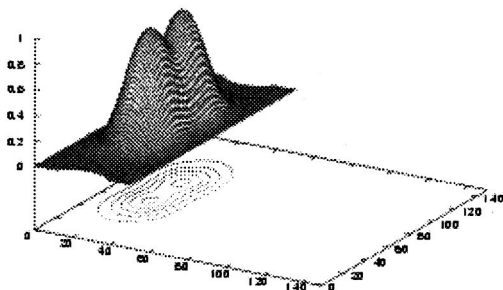
Figure 36. The initial concentration distribution for the stream.



a) after 25 s



b) 60 s



c) 90 s

Figure 37. The evolution of the stream.

Observations

These preliminary simulations demonstrate two interesting phenomena for miscible fluids. An aspherical drop can become spherical as would be seen for immiscible fluids. A stream has a tendency to break up via a Rayleigh-like instability but does not completely, probably because the effective interfacial tension relaxes with time. Moreover, it begins to split but after some time the splitting stops, and the tendency is rather opposite -- to form a single, probably spherical, drop. More simulations will be required to elucidate the long-term behavior.

More simulations....

In 2002 we used an adaptive grid formulation to explore three situations. The first case will involve a variation in the width of the transition zone across the grid. Secondly we will explore an interface of constant width, with a linear temperature gradient parallel to the interface. The third case we will investigate deals with a constant transition zone width, no applied temperature gradient, however there will be a gradient in the percent polymer conversion parallel to the interface. This corresponds to a variation in concentration. In addition, conversion and temperature are linked since complete conversion can increase the temperature by 150 K.

Variable Transition Zone Width

In this section we will explore fluid flow induced by creating a variable transition zone width across the grid. There are two possible situations: one where the width of the transition zone is independent of location, the other where the transition zone width is a function of the location. Figure 38 demonstrates a variable transition zone.

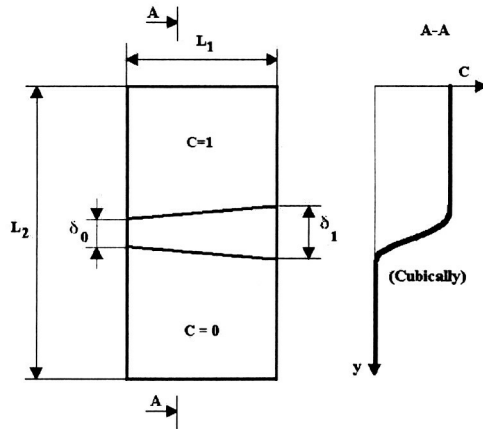


Figure 38. The configuration of the simulations with the variation in the width of the transition zone.

For the above configuration we explored fluid flow under several conditions. We allowed for variations in the square gradient parameter as well as variations in the overall width. Figure 39 demonstrates the fluid displacement and the streamlines after 1000 seconds for a transition zone width increasing from 0.2-5 mm and with $k = 2 \times 10^{-9}$ N.

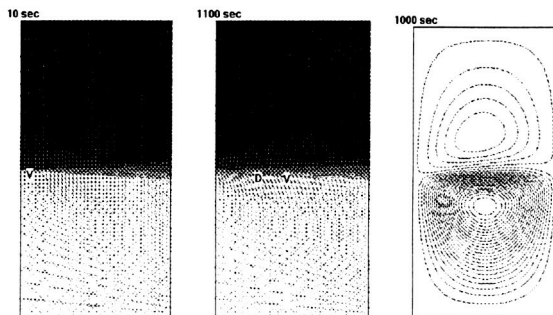


Figure 39. Simulation with a variable transition zone: δ from 0.2 mm to 5 mm with $k = 2 \times 10^{-9}$ N. Polymer concentration is indicated by the gray level.

Utilizing the same model but varying the width of the transition zone and k , indicates several interesting points. First of all the overall displacement increases with increasing variations in the transition zone width. Also the overall displacement increases as a function of k . What's interesting is that the overall displacement increases asymptotically with the overall difference in the transition zone width, approaching a maximum displacement for a variable transition zone from 0.2-5 mm. This can be seen in Figure 40.

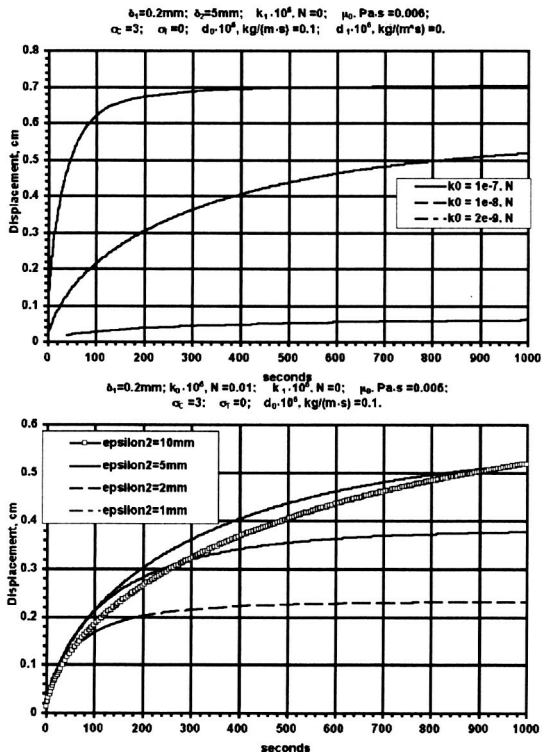


Figure 40. Top: The maximum displacement of fluid as a function of time for different values of k . Bottom: The maximum displacement for different values of the transition width variance.

Figure 40 shows that the ideal case to be studied is one with a large value for the square gradient parameter and a transition zone width increasing from 0.2-5 mm.

Linear Temperature Gradient

We modeled a uniform concentration gradient (constant δ) with a linear temperature gradient parallel to the interface. We studied many cases but we discuss two here. First, we used eq. 6 to estimate the temperature-dependence of k . In addition we include a variable viscosity, increasing to 0.3 Pa s after 10000 seconds. Using this value and applying a temperature difference along the transition zone of 50 K, we predicted a very weak fluid flow. Figure 41 demonstrates the flow resulting from such a situation.

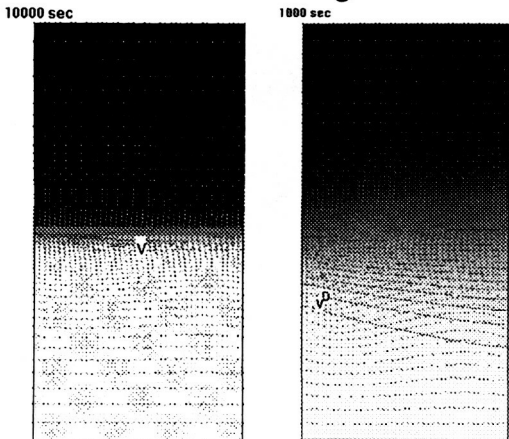


Figure 41. Left: The effect of a variation in k from 1.5×10^{-9} N to 1.7×10^{-9} N with $\mu = 0.002$ Pa s increasing to 0.3 Pa s, after $10,000$ s. Right: With k independent of T , $k = 10^{-9}$ N but the diffusion coefficient increasing four times from right to left, after 1000 s.

However, by imposing a temperature gradient, we also change the diffusion coefficient along the transition zone. We estimate that a 50 K gradient in temperature will cause the diffusion coefficient to increase 4-fold along the transition zone. The fluid flow induced by the gradient in the diffusion coefficient is much more pronounced. Figure 41 depicts fluid flow with a square gradient parameter independent of the applied temperature gradient. The predicted fluid flow is due only to the gradient in the diffusion coefficient.

The presence of fluid flow due to temperature dependent diffusion coefficients is important. Theoretically k should increase with temperature however, the temperature dependence of k , has not yet been experimentally proven. Whether k increases or decreases with temperature determines the direction of fluid flow on the grid. Thus it is possible that the temperature dependence of k and the temperature dependence of the diffusion coefficient would produce counteracting fluid flow. In addition we have shown that even for a weak temperature dependence of k , fluid flow will occur solely due to the change in the diffusion coefficient.

Conversion Gradient

Imposing a compositional gradient along the interface results in several additional variations. First of all the temperature will also vary. As the polymer forms heat is released to the surroundings, therefore in regions of high polymer conversion the temperature will be high, in regions of low polymer conversion the temperature will be low. As was seen in the previous model, a variation in temperature results in a variation in the square gradient parameter and also the diffusion coefficient.

We first consider a simplified system, where a conversion gradient exists, resulting in a variable temperature. We will assume viscosity is independent of temperature and neglect the change in the diffusion coefficient.

Figure 42 demonstrates such a system with a $k = 1 \times 10^{-8}$ N, a conversion gradient from right to left of 0 - 100% , and a temperature variation from 25 - 150 K.

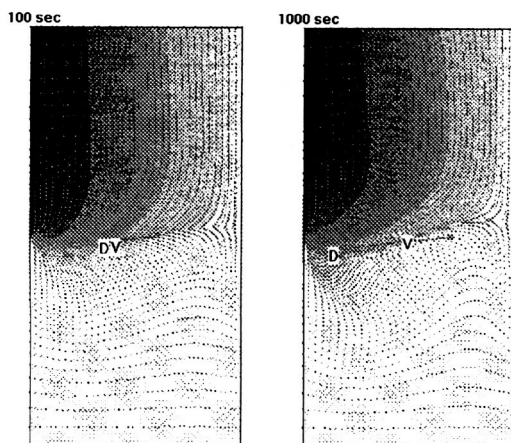


Figure 42. Left: Flow fields for conversion gradient after 100 seconds. Right: After 1000 seconds.

Such a system results in significant fluid flow. Figure 42 demonstrates the maximum displacement of a particle as a function of time. For the system outlined in Figure 41, a maximum displacement of 1.6 cm can be obtained after 1000 seconds.

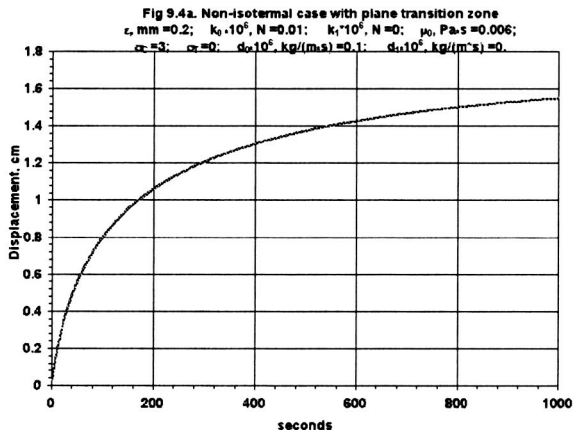


Figure 43. Maximum Displacement as a function of Time.

Now lets look at a system with a conversion gradient like that outlined in Figure 42 with a temperature dependent diffusion coefficient and a constant k. Figure 43 shows the flow fields for a conversion gradient system with $k=1 \times 10^{-8}$ N, a diffusion coefficient increasing from 1×10^{-6} - 1.2×10^{-5} cm/s from right to left, and a temperature increasing from right to left from 25-150 K.

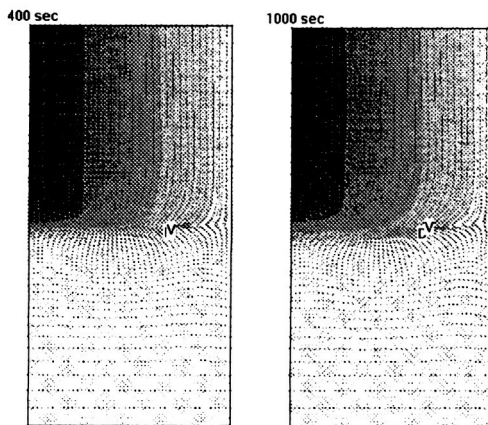


Figure 44. Left: Flow field after 400 seconds. Right: Flow field after 1000 seconds.

Including a temperature-dependent diffusion coefficient results in competing flow fields. These result in a decreased particle velocity, and correspondingly a decrease in the maximum displacement. A plot of the maximum displacement shows that assuming a temperature dependent diffusion coefficient results in decreased but still measurable fluid flow. Figure 45 shows that a maximum displacement of approximately 0.37 cm is obtained after 1000 seconds.

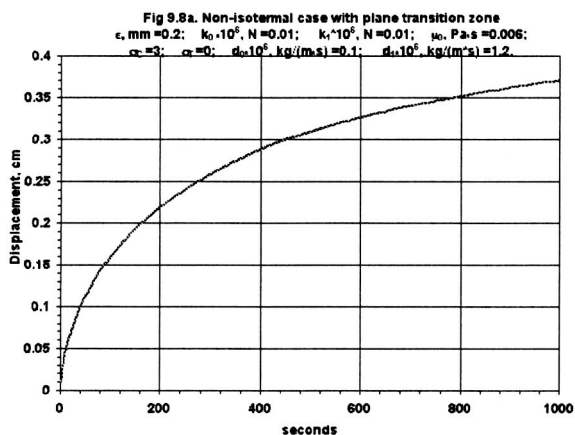


Figure 45. Maximum Displacement of a system containing a conversion gradient with constant k and temperature dependent diffusion coefficients.

Flow for Low Values of K

Thus far we have shown that measurable fluid flow can be achieved for the three types of experiments we propose. It can also be shown that measurable fluid flow can even be observed for square gradient terms approaching $1 \times 10^{-11} \text{ N}$.

We consider a system with a temperature gradient. We will assume that both the square gradient term and the diffusion coefficient are temperature dependent. Figure 46 depicts the flow fields for a system with k increasing from 4×10^{-11} to $6 \times 10^{-10} \text{ N}$. In addition the diffusion coefficient will increase from 1×10^{-6} to $1.2 \times 10^{-5} \text{ cm/s}$.

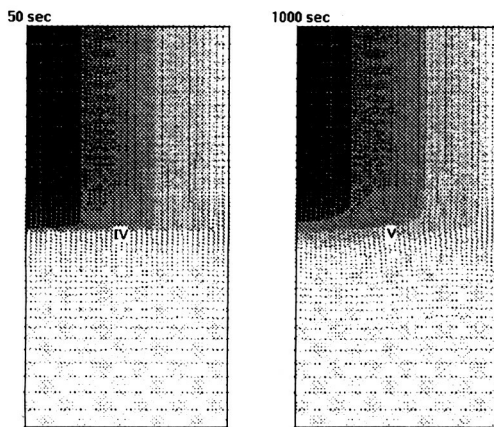


Figure 46. Left: Flow field for low k after 50 sec. Right: Flow field for low k after 1000 seconds.

Although significantly weaker flow fields result, plots of maximum displacement as a function of time indicate measurable fluid flow. Figure 47 shows that after 1000 seconds a maximum displacement of 0.05 cm develops.

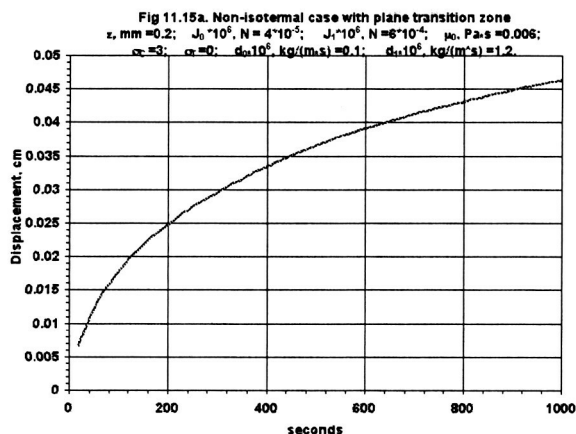


Figure 47. Maximum displacement for a system with k approaching $1 \times 10^{-11} \text{ N}$.

Qualitative Experiments

Due to the small fluid flows caused by compositional gradients it is possible that we will not be able to completely separate fluid flow due to compositional gradients from fluid flow due to residual gravity. For this reason it would be desirable to develop an experiment that could determine the presence of compositional gradient induce fluid flow based on qualitative measurements.

A recent numerical simulation elucidated such an experiment. By setting up a non-linear variable transition zone width interesting fluid flow results. Two variations in the transition width will be considered. The first will consist of an equal transition zone width at each edge of the grid, with a decreasing transition zone width towards a minimum at the center. The other will consist of an equal transition zone width at each edge of the grid with an increasing transition zone width towards a maximum in the center. We will define the transition zone width with three quantities, the left edge, ϵ_1 , the right edge, ϵ_2 , and the center, ϵ_3 . We will also assume that the temperature field is uniform along the interface and hence k and the diffusion coefficient are constant.

Figure 48 depicts the resulting fluid flow for a system with $\epsilon_1 = \epsilon_2 = 5 \text{ mm}$ and $\epsilon_3 = 0.2 \text{ mm}$. We have assumed a constant $k = 1 \times 10^{-9} \text{ N}$, and a constant diffusion coefficient of $1 \times 10^{-6} \text{ cm/s}$.

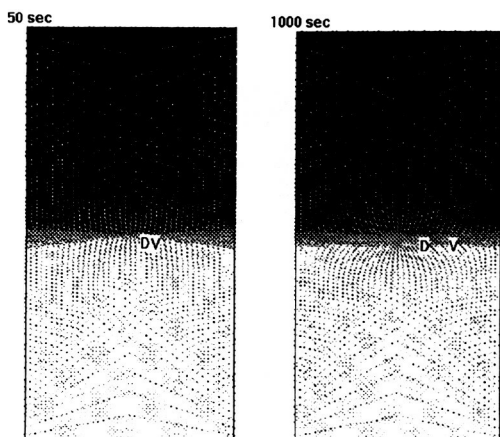


Figure 48. Flow fields for non-linear variations in the transition zone width. Width decreases from sides to the middle of the grid. Left: After 50 seconds. Right: After 1000 seconds

The result essentially breaks down the fluid flow into quadrants. The flow goes from regions of large transition zone width to regions of small transition zones. The result is opposing flows in both the polymer rich region and the monomer rich region. This eliminates the complications in using quantitative measurements to verify the effect of conformational gradients.

The second case we will examine compliments the qualitative approach to verifying the effect of compositional gradients on fluid flow. In this case we set $\epsilon_1 = \epsilon_2 = 0.2$ mm and $\epsilon_3 = 5$ mm. Again we have assumed a constant $k = 10^{-9}$ N, and a constant diffusion coefficient of 10^{-6} cm/s. Now the transition zone width is at a minimum at the walls and a maximum at the center. However, we still observe fluid flow from regions of large transition zone width to regions of small transition zone width. Therefore the observed fluid flow in Figure 49 is exactly opposite the case observed in Figure 48.

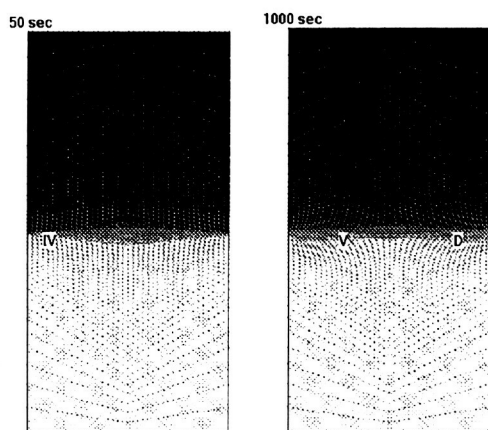


Figure 49. Flow fields for non-linear variations in the transition zone width. Width increases from the sides to the middle of the grid. Left: After 50 seconds. Right: After 1000 seconds

Despite providing a qualitative example of compositional gradient induced fluid flow, it is still necessary to have measurable fluid flow in order to deduce the direction of flow in the system. We conducted the above sets of experiments for $k = 10^{-9}$ N, $k = 10^{-10}$ N, and $k = 10^{-11}$ N. All demonstrate the same qualitative fluid flow as depicted in Figure 48 and Figure 49. As expected the magnitude of fluid flow decreases with decreasing k . Figure 50 depicts the maximum displacement as a function of time for a system with $\epsilon_1 = \epsilon_2 = 0.2$ mm and $\epsilon_3 = 5$ mm for various values of k .

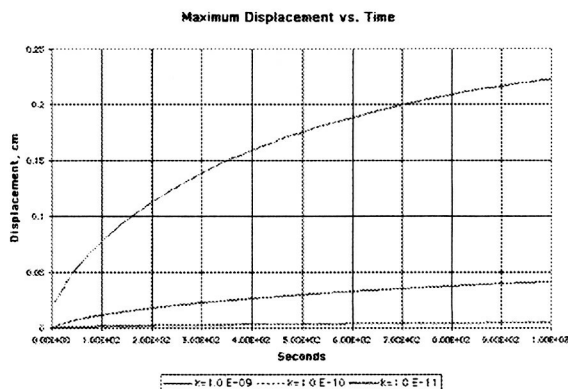


Figure 50. Variation in maximum displacement with decreasing values of k .

As can be seen from the plot above a minimum displacement of 0.0045 cm after 1000 seconds is obtained with a $k=1.0 \times 10^{-11}$ N. This increases to 0.22 cm for a $k=1.0 \times 10^{-9}$ N. Although the total fluid displacements are small discernable distortions to the concentration field should be observed with optical techniques.

The total fluid flow for the case with $\epsilon_1=\epsilon_2=5$ mm and $\epsilon_3=0.2$ mm yielded similar order of magnitude total fluid displacements, as can be seen in Figure 51.

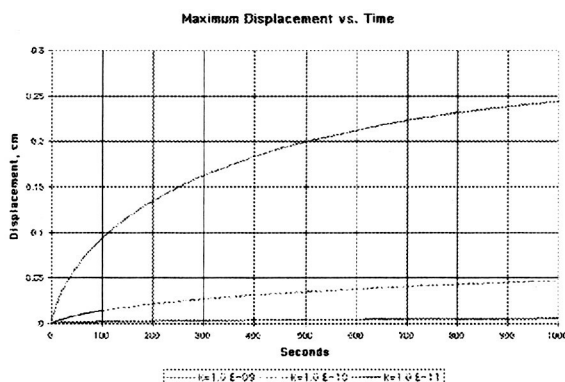


Figure 51. Variation in maximum displacement with decreasing values of k .

Figures 50 and 51 demonstrate that measurable fluid flow can be observed for all values of k that we have predicted. Therefore the presence of qualitatively different flows in using a non-linear variable transition zone widths proves the last case to be experimentally useful.

Conclusions

Using our Korteweg stress model with variable coefficients and an adaptive grid we were able to demonstrate measurable fluid flow for three cases: One in which there was a variable transition zone width, one with a temperature gradient and one with a gradient of polymer conversion.

Several important insights were elucidated during the modeling. First of all coupling a temperature gradient with the corresponding gradient in diffusion coefficients yielded interesting flow patterns. In the case of a temperature variation induced by a conversion gradient, fluid flow

due to variable diffusion coefficients and variations in conversion produced counteracting flow fields.

Also of interest was the influence of non-linear variable transition zone widths. By creating variable transition zones, which were symmetric about the center of the grid we were able to show opposing flow fields in the grid. These simulations resulted in qualitatively different flow fields induced by compositional gradients.

Of principle importance we were able to show that readily discernable distortions to the concentration field occur in systems with square gradient parameters as low as 1×10^{-11} N. This limit indicates that all our predicted possible values of the square gradient term will result in measurable fluid flow.

Spinning Drop Tensiometry

In 2002 we continued our study of miscible fluids with tensiometry. We used a spinning drop tensiometer to explore miscible fluid behavior in order to estimate the value of the square gradient parameter, k . Two differences exist in studying miscible systems instead of the traditional immiscible systems. First of all a miscible system by definition cannot possess a real interface or interfacial tension. However, for the purposes of this paper we will use the term "interface" to define the transition zone between two miscible fluids. Assuming an interfacial tension of zero would imply that the drop should relax to an infinite length of zero radius when rotated. Without a counteracting interfacial force the drop would approach the mechanically stable situation with the less dense solution occupying the region closest to the rotational axis. Previous work by Pojman et al.⁸⁴ has demonstrated that a miscible drop will reach a quasi-steady non-zero radius. Likewise Petitjeans⁸¹ used spinning drop tensiometry to measure the EIT of a glycerin/water system to be 0.58 ± 0.07 mN/m. However, the presence of a quasi-steady radius is not necessary and sufficient information for an actual EIT. The systems studied thus far have used a viscous medium for the bulk fluid. The influence of viscosity on miscible drop relaxation has not been explored. In addition diffusion also plays a role in the equilibrium shape of a miscible drop. Therefore one must determine a method to separate diffusive effects from viscous relaxation effects.

Previous experiments did not measure the rate of rotation dependence or the width of the transition zone, which is a crucial parameter necessary to estimate the square gradient parameter. In this study we determined the effect of viscosity on the relaxation profile of a miscible drop. In addition the rotational dependence of the EIT was determined. Finally, an estimation of the square gradient parameter was obtained.

Experimental

Poly(dodecyl acrylate), PDDA, was used throughout the experimental studies. Dodecyl acrylate (DDA), obtained from Sartomer, was photo-polymerized at 365 nm using an EFOS mercury lamp with an intensity of 76 mW/cm^2 for 30 minutes under constant stirring. The monomer solution contained 3 mM Irgacure 184, as a photoinitiator, and 2.0% dodecyl mercaptan as a chain transfer agent.

The resulting PDDA was characterized by determining the density in order to confirm near complete conversion. The density measurements were recorded to 5 significant figures using a Paar DMA 4500 densitometer.

All surface tension studies were conducted using a Krss Site 4 spinning drop tensiometer (SDT). An oil bath circulator was used to maintain a constant temperature of 27 ± 1 °C. In order to compensate for the optical effects induced by the Plexiglas windows, circulating oil, and polymer a calibration procedure was used. All measurements conducted upon images obtained using spinning drop tensiometry used the same calibration procedure. A metal rod of known diameter was inserted into the capillary. An image of the rod was then obtained and the diameter was recorded. The known diameter was then related to its diameter in pixels.

In order to image the drop, a dye, Zinc meso-tetraphenylporphine was used. The dye was added to the monomer, which was injected into the bulk polymer fluid. The drop was then illuminated using an 8-mW laser line projector. All images were obtained using a CCD camera mounted perpendicular to the illumination. An additional camera, a Sony digital camcorder with dioptic lenses was also mounted perpendicular to the illumination in order to observe the length of the drop. The resulting images were then analyzed using imaging software.

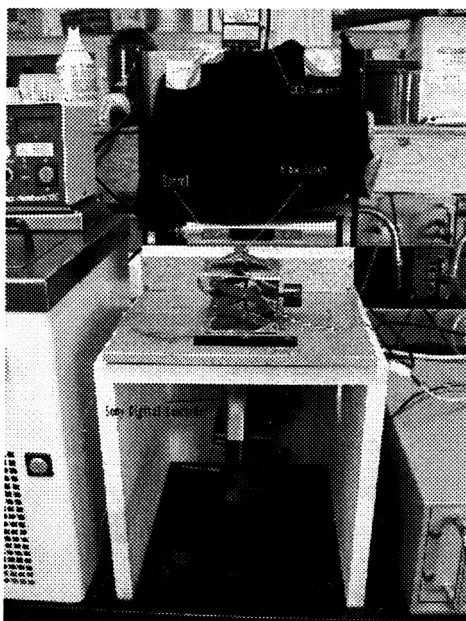


Figure 52. Experimental Apparatus
Imaging

One of the fundamental aspects of this project involved defining the “interface.” Since we were dealing with miscible fluids, a true interface did not exist, but rather a transition from monomer rich regions (the drop), to polymer rich regions. We defined the interface by obtaining a cross section of pixel intensity across the raw image, Figure 53.

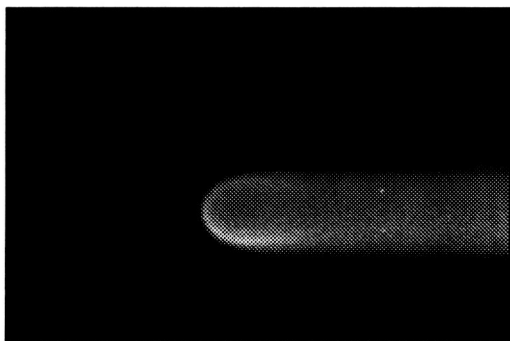


Figure 53. Raw image of PDDA/DDA after 500 seconds. Drop diameter is 0.5 mm.

Figure 54, demonstrates the resulting pixel intensity cross section of the drop. We defined the drop interface as the point at which the pixel intensity deviates from the maximum. Thus the drop diameter is bounded by sub-maximum pixel intensities. Similarly we were able to define the width of the transition zone from Figure 54.

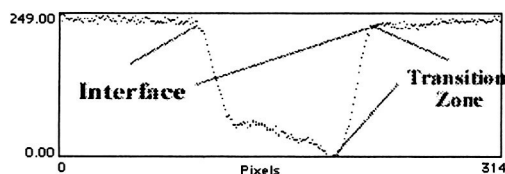


Figure 54. Pixel intensity cross section profile of PDDA/DDA after 500 seconds.

Figure 54 shows three regions of interest. The region with maximum pixel intensity contains minimal dye and consequently only minimal monomer. Thus this region is our polymer rich region. The region with the minimal pixel intensity contains the maximum amount of dye, and therefore is our monomer rich region. The deviation from a slope of zero in this region is a consequence of a drop off in light intensity across the capillary. The final region consists of the sloped regions. These regions consist of a gradient in concentration of dye, and hence monomer. Therefore this region is the transition zone we are interested in. We will define the width of the transition zone, δ , as the width of this region.

Results

Our first goal was to verify evidence suggesting the presence of an actual EIT. Initial experiments with a dodecyl acrylate/poly (dodecyl acrylate) system demonstrated that the drop reached a quasi-steady radius. Figure 55 shows that after approximately 100 seconds the drop diameter is not substantially different than the diameter after 1000 seconds. The existence of a quasi-steady nonzero radius suggests that an actual effective interfacial tension may exist and can be measured with a SDT. The possibility of an actual EIT provided motivation for further study of miscible interfacial phenomena with a SDT. However, it is possible that the viscosity of the polymer inhibits the relaxation profile of the drop.

Long relaxation times have been observed for high viscosity polymer melts.^{79, 85, 86} These large relaxation times can inhibit accurate measurements of interfacial tensions. Joseph et al.^{79, 85, 86} demonstrated that rotation jumps in high viscosity fluids could be used to determine an accurate estimate of an interfacial tension. He demonstrated that the relaxation profile of a drop

in a high viscosity fluid is exponential. Using this concept we can estimate the viscous relaxation time for our polymer by determining the relaxation profile for an immiscible system, containing our polymer as the bulk fluid, that would be analogous to our miscible system.

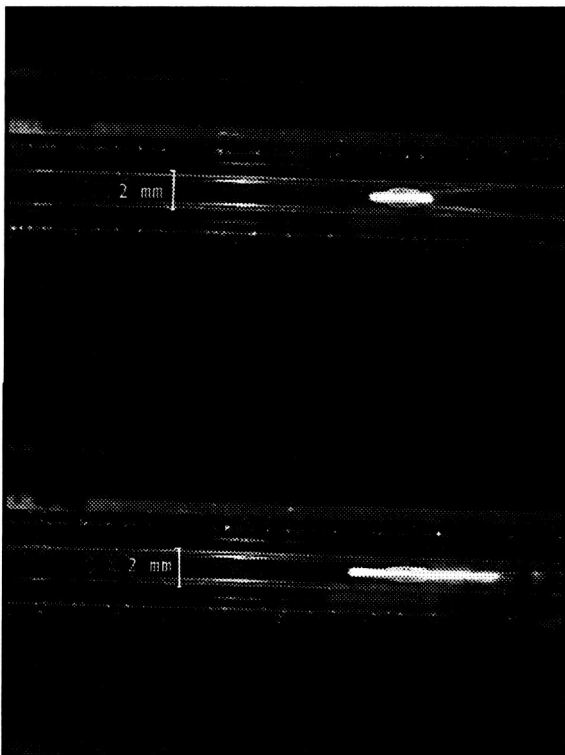


Figure 55. Top: Drop of DDA in PDDA rotated at a rate of 2000 RPM after 100 seconds. Bottom: Drop of DDA in PDDA after 1000 seconds. Scale: The capillary width is 2.0 mm.

In finding an immiscible analog, several parameters are important. A large interfacial tension implies a quick relaxation time, since the equilibrium shape is not substantially different than the initial shape. Therefore, the interfacial tension needs to be approximately the same as the value expected for the EIT. Secondly, the density of the immiscible drop must be less than the density of the polymer. In addition to these two conditions, the difference in densities between the drop and bulk fluid should also be held as close as possible to that of the miscible system being studied.

The small carbon chain alcohols, methanol, ethanol, and propanol are all insoluble or only partially soluble in PDDA and have densities less than that of our polymer. In analyzing their properties, propanol was determined to be best suited as an immiscible analog. Since propanol is partially soluble in PDDA, one must first saturate both the PDDA and propanol to avoid relaxation of the drop due to diffusion.

Table 1 Critical Parameters for Immiscible Analog

Species	Density at 25	Estimated IT or EIT	Difference in Density for
---------	---------------	---------------------	---------------------------

	degrees Celsius (g/mL)	(mN/m)	system (g/mL)
Propanol*	0.80913	0.43	0.10162
Poly (dodecyl acrylate) saturated with propanol	0.91075		
Dodecyl acrylate	0.87643	>0.06	0.05474
Poly (dodecyl acrylate)	0.93117		

*Propanol was saturated with polymer before density was obtained.

Table 1 demonstrates that propanol is a suitable choice for an immiscible analog. Its interfacial tension of 0.43 mN/m is below the EIT of glycerin/water measured by Petitjeans using a SDT.⁸¹ Therefore, the relaxation behavior should be on the same time scale. In addition, the density difference is small and of a similar magnitude. Since, the difference in density is also a driving force in the attainment of an equilibrium shape it is necessary for the immiscible analog to have a similar density difference. Therefore, a saturated propanol system can be used as an immiscible analog.

The relaxation time for the immiscible analog was estimated by subjecting the propanol drop to a series of rotation jumps. Two types of rotation jumps were conducted, one from a high rate of rotation to a lower rate of rotation, and the other from a low rate of rotation to a high rate of rotation. The plots observed in Figure 5 demonstrate the relaxation behavior.

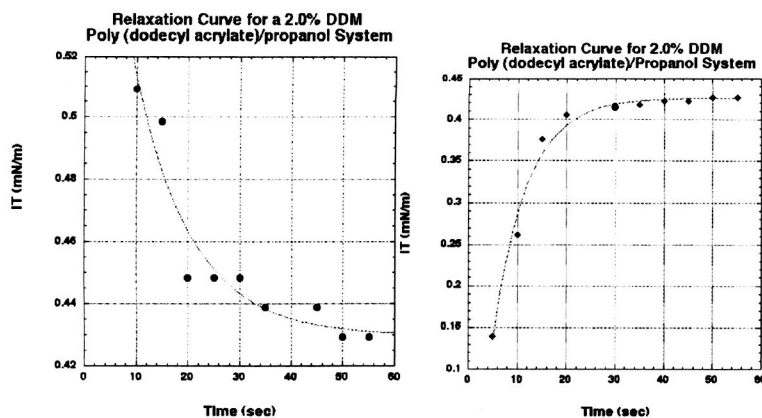


Figure 56. Left: Relaxation profile for low-high rate of rotation. Right: Relaxation profile for high-low rate of rotation.

Both relaxation curves exhibit an exponential decay. This is exactly what Joseph has published for viscous relaxation in immiscible systems. In addition, both reach the same

asymptotic value of 0.43 mN/m. The relaxation time can be taken as the amount of time necessary for the drop to reach the asymptotic IT. In these cases it can be estimated at 50 seconds. This value is well within the time capabilities of our system. However, since our systems difference in density as well as EIT are less than those for the immiscible analog we should expect a larger relaxation time. It will be assumed to be on the order of 100 seconds.

Rate of Rotation Analysis of PDDA/DDA

One of the characteristics of using spinning drop tensiometry to measure IT's, in immiscible systems, is that above a critical rate of rotation the observed value for the IT does not depend upon the rate of rotation. The rate of rotation dependence below this critical value has been studied. The primary problems at low rotations were reported by Currie⁸⁷ to be due to buoyancy effects. These effects lead to non-cylindrical shaped drops. Princen *et al.*⁸⁸ and Slattery and Chen⁸⁹ have developed more sophisticated methods to determine the IT for non-cylindrical drops.

One of our goals was to determine whether a critical rate of rotation exists for our miscible PDDA/DDA system. Several rates of rotation were studied, ranging from 2000 RPM to 8000 RPM. A plot of the time dependent EIT is plotted for various rates of rotation in Figure 57.

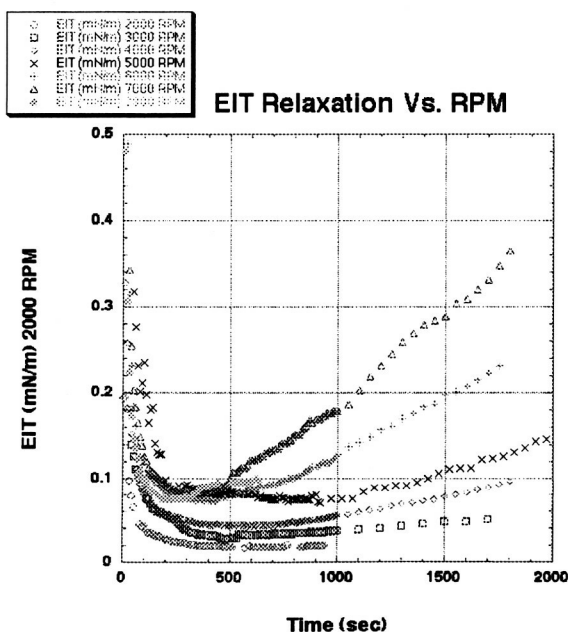


Figure 57. Plot of EIT relaxation profile for varying rates of rotation.

There are several immediate observations from Figure 57. First of all, there is a clear increase in the EIT at longer time scales. The incidence of this increasing EIT occurs earlier for increasing rates of rotation. The occurrence of an increasing EIT can be attributed to the effect of diffusion on a miscible system. The effects of diffusion cannot readily be seen until after the viscous relaxation time period. The viscous relaxation should occur faster in the presence of a larger rotational force, thereby allowing the diffusive effects to play a role at earlier time scales.

The second observation is that the EIT does show a direct relationship between the rate of rotation and the EIT. In addition, for the rates of rotation of 5000, 6000, 7000, and 7900 the value for the EIT from 250 seconds to 500 seconds are approximately equal. This is the

approximate the time at which the system has relaxed completely. The presence of equal asymptotic values for the EIT at varying rotation rates indicates that a critical rate of rotation may also exist for miscible systems. In order to obtain a clearer depiction of the critical rate of rotation, we prepared a plot of the asymptotic EIT vs. the rate of rotation.

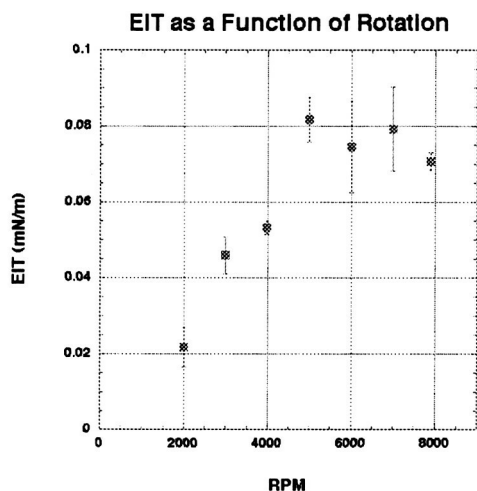


Figure 58. Plot of asymptotic EIT for varying rates of rotation.

Figure 58 clearly depicts the presence of an asymptotic EIT of approximately 0.08 ± 0.01 mN/m above a rate of rotation of 5000 RPM. Therefore, two conclusions can be made. First of all, a critical rate of rotation does exist for the PDDA/DDA system. In addition, above 5000 RPM an EIT of 0.08 ± 0.01 mN/m is obtained. This value for the EIT will be used in all further calculations.

Estimation of the Square Gradient Parameter:

By measuring both the EIT and width of the transition zone as a function of time, we were able to estimate the square gradient parameter. Figure 8 demonstrates the variation of the square gradient parameter with time.

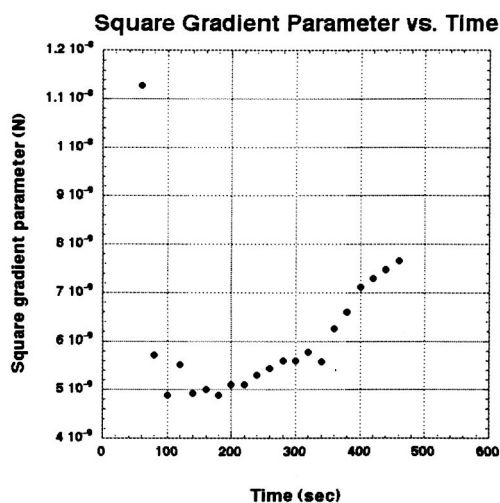


Figure 59. Time profile of the square gradient parameter.

Figure 59 clearly depicts the square gradient parameter to be on the order of $5-8 \times 10^{-9}$ N. The plot also suggests that the square gradient parameter increases with time. However, this is most likely an artifact of the way we defined the interface. Since, our data shows that the EIT increases with time due to diffusion, it would be expected that the square gradient parameter, a function of EIT, would also increase with time. Likewise due to our definition of the interface, the width of the transition zone would be expected to increase with time. Thus, our plot is consistent with our expectations, and gives us an estimate of the square gradient within an order of magnitude.

Estimation of the Square Gradient Parameter

The second technique utilized thermodynamic theories which have shown that the square gradient parameter was related to the radius of gyration, R_{gyr} , the molar volume of the solvent, V_{molar} , and the Flory-Huggins interaction parameter, X . The factor RT is included to yield the enthalpy of mixing.⁹⁰

$$k = \frac{R_{gyr}^2 RTX}{3V_{molar}}$$

We can estimate X for a good solvent to be approximately 0.5. In our case the solvent is the monomer, which has a molar volume of $2.7 \times 10^{-4} \text{ m}^3 \text{ mole}^{-1}$. The radius of gyration is more difficult to estimate. It can be determined directly from light scattering, however initial attempts have proven difficult. A crude approximation can be obtained from a unification of gel permeation chromatography (GPC) theory and light scattering.

In obtaining the molecular weight of our polymer with a GPC, what we measure is the molecular weight of a polystyrene molecule with the same hydrodynamic radius as our polymer. The hydrodynamic radius is related to the radius of gyration. Therefore we can determine the MW dependence of polystyrene's radius of gyration and obtain a plot of the square gradient parameter as a function of MW. The result indicates that the square gradient parameter varies from 10^{-11} - 10^{-9} N for MW from 10^4 - 10^6 .

It is our goal to demonstrate that within the range of 10^{-11} - 10^{-8} N, we can obtain measurable fluid flow.

Conclusions from our SDT Studies

Using spinning drop tensiometry the interfacial properties of a PDDA/DDA system were measured. The results are more accurate than our preliminary work with the high temperature SDT of Joseph because of superior imaging but the experiments were performed at lower temperatures.

The time dependence of the EIT was determined to follow a three fold path. The first due to viscous relaxation effect, depicts a pattern consistent with exponential decay. The second corresponds to the equilibrium EIT and radius and is observed as the asymptotic value associated with the exponential function. The third aspect of the time dependence of EIT was growth due to diffusion.

In studying the relaxation of a PDDA/DDA system an asymptotic EIT of 0.08 ± 0.01 mN/m was obtained. The corresponding transition zone width was approximately 0.10 mm yields an approximate square gradient parameter of 8×10^{-9} N. This value corresponds well to the time dependence of the square gradient parameter. Therefore the approximate square gradient parameter is on the order of $5-8 \times 10^{-9}$ N.

Comparing this value with the results from the numerical approach indicates that spinning drop tensiometry yields consistently larger values for the square gradient parameter. It should be noted that to our knowledge no one has measured a square gradient parameter for a miscible system. In addition the numerical approach utilizes several approximation. Despite the difficulties a unification of the two approaches can yield an upper and lower limit for the square gradient parameter. From our studies we can take this range to be 10^{-11} - 10^{-8} N.

Fluorescence Studies

Many studies have been done using fluorescence probes to monitor polymerization.⁹¹⁻⁹⁶ However, we no of no result of using fluorescence to measure viscosity during a polymerization with temperature polymer concentration chaning. The goal of the study was to determine whether fluorescence could be used to monitor viscosity. We also had to confirm that the method is independent of temperature and molecular weight of the polymers. The fluorescence measurements were performed by Pat Bunton at William Jewel College.

We tested pyrene as a probe of viscosity to determine if there is a correlation between viscosity and fluorescence for a given temperature. However, at high molecular weights, results were different in that for the pure polymer, the curve digresses from the standard curve. Figure 60 shows the graph of normalized fluorescence vs. viscosity for both the high and low molecular weights.

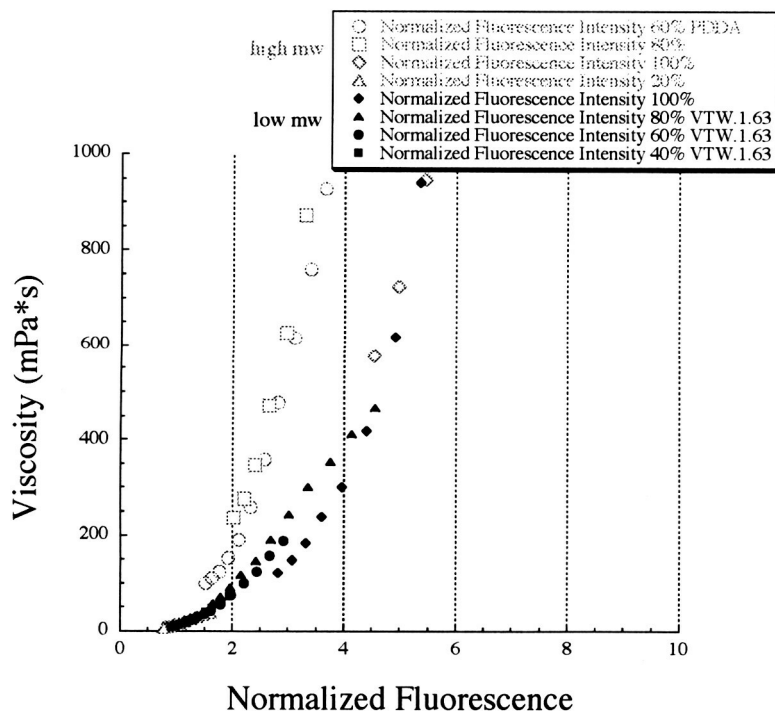


Figure 60. Graph of Fluorescence vs. Viscosity for Low and High Molecular Weights.

Pyrene was used in this experiment as the molecular probe. Normalized fluorescence measurements at 388nm were performed as a function of temperature. Viscosity of poly (dodecyl acrylate) at various concentrations was measured. These results were compared.

Conclusions

We traversed a mighty journey—starting with frontal polymerization and ending up with fundamental studies of miscible fluids. We were able to answer all but one essential question using frontal polymerization on the ground or KC-135 flights. Determining how effective interfacial tension can affect FP is premature until we know if such an effective interfacial tension exists and if so, how important it can be in miscible polymer/monomer systems. The TIPMPS flight project will enable us to answer that question.

“Keep your feet in the lab but keep reaching for the stars.”

Publications

Chekanov, Y., Pojman, J.A., and Rasmussen, J.K. Bubble-free initiators for high temperature free-radical polymerization. *Polym. Prep. Am Chem. Soc. Div. Polym. Chem.*, 39 (2), 465 (1998).

Lewis, L.L., and Pojman, J.A. Experimental investigation of the mechanism of isothermal frontal polymerization. *Polym. Mater. Sci. Eng. Prep. Div. Polym. Mater. Sci. Eng.*, 78 (1), 38-39 (1998).

Lewis, L.L., Pojman, J.A., Owens, J., and Coleman, J. An experimental investigation of the mechanism behind isothermal frontal polymerization. *Polym. Mater. Sci. Eng. Prep. Div. Polym. Mater. Sci. Eng.*, 79, 44-45 (1998).

Masere, J., and Pojman, J.A. Period-doubling behavior in propagating fronts of multifunctional acrylates. *Polym. Mater. Sci. Eng. Prep. Div. Polym. Mater. Sci. Eng.*, 79, 80-81 (1998).

Masere, J., Pojman, J.A. Free radical-scavenging dyes as indicators of frontal polymerization dynamics. *J. Chem. Soc. Faraday Trans*, 94, 919-922 (1998).

McCaughey, B., Pojman, J.A., Simmons, C., Volpert, V.A. The effect of convection on a propagating front with a liquid product: comparison of theory and experiments. *Chaos*, 8, 520-529 (1998).

Pojman, J.A., Griffith, J., and Simmons, C. Binary frontal and frontal copolymerization. *Polym. Prepr. Am Chem. Soc. Div. Polym. Chem*, 38 (1), 231-232 (1998).

Pojman, J.A., Gunn, G., Patterson, C., Owens, J., Simmons, C. Frontal dispersion polymerization. *J. Phys. Chem. B*, 102, 3927-3929 (1998).

Pojman, J.A., Nichols, H.A., and Volpert, V. The effects of reactor orientation on frontal polymerization. *Polym. Prep. Am Chem. Soc. Div. Polym. Chem*, 39 (2), 463-464 (1998).

Pojman, J., Chekanov, Y.A., Case, C., and McCardle, T. Functionally-graded polymeric materials prepared via frontal polymerization. *Polym. Mater. Sci. Eng. Prep. Div. Polym. Mater. Sci. Eng.*, 79, 82-83 (1998).

Masere, J., Stewart, F., Meehan, T., and Pojman, J. A. Period-doubling behavior in frontal polymerization of multifunctional acrylates. *Chaos*, 9, 315-322 (1999).

Pojman, J.A. Self organization in synthetic polymeric systems. *Annals New York Acad. Sci.*, 879, 194-214 (1999).

Pojman, J.A. and Epstein, I.R. Nonlinear chemical dynamics in polymeric systems. *Chaos*, 9, 255-259 (1999).

Pojman, J.A., Fortenberry, D., Lewis, L.L., Simmons, C., Ilyashenko, V. "Solvent-Free Synthesis by Free-Radical Frontal Polymerization": in "Solvent-Free Polymerizations and Processes." Edited by: Long, T. E. Hunt, M. O., ACS Symposium Series No. 713; American Chemical Society: Washington, D.C., pp 140-153, 1999.

Fortenberry, D.I., and Pojman, J.A. Solvent-free synthesis of polyacrylamide by frontal polymerization. *J. Polym. Sci. Part A: Polym Chem.*, 38, 1129-1135 (2000).

Texier-Picard, R., Pojman, J.A., Volpert, V.A. Effect of interfacial tension on propagating polymerization fronts. *Chaos*, 10, 224-230 (2000).

Downey, J. P.; Pojman, J. A. (editors) "Polymer Research in Microgravity: Polymerization and Polymer Processing", ACS Symposium Series No. 793, American Chemical Society: Washington, D.C, 2001.

Downey, J. P.; Pojman, J. A. "Polymer processing in microgravity -- An overview" in "Polymer Research in Microgravity: Polymerization and Polymer Processing", Downey, J. P.; Pojman, J. A. (editors), ACS Symposium Series No. 793, American Chemical Society: Washington, D.C, pp 2-15 2001

Ainsworth, W.; Pojman, J. A.; Chekanov, Y.; Masere, J. "Bubble behavior in frontal polymerization: Results from KC-135 parabolic flights" in "Polymer Research in Microgravity: Polymerization and Polymer Processing", Downey, J. P.; Pojman, J. A. (editors), ACS Symposium Series No. 793, American Chemical Society: Washington, D.C, pp 112-125, 2001

Pojman, J. A. Nonlinear chemical dynamics in synthetic polymeric systems: motivations and strategies for success. *Macromolecular. Symposia*, 160, 207-214 (2000)

Manz, B., Masere, J., Pojman, J. A., and Volke, F. Magnetic resonance imaging of spiral patterns in crosslinked polymer gels produced via frontal polymerization, *Journal of Polymer Science Part A. Polymer Chemistry*, 39, 1075-1080 (2001)

Masere, J., Chekanov, Y., Warren, J. R., Stewart, F., Al-Kaysi, R., Rasmussen, J. K., and Pojman, J. A. Gas-free initiators for high-temperature polymerization. *Journal of Polymer Science Part A. Polymer Chemistry* 38, 3984-3990 (2000)

Masere, J.; Lewis, L. L.; Pojman, J. A. Optical gradient materials produced via low-temperature isothermal frontal polymerization. *Journal of Applied Polymer Science* 80, 686-691 (2001)

Allali, K., Pojman, J., and Volpert, V. Influence of vibrations on convective instability of polymerization fronts. *Journal of Engineering Mathematics* 41, 13-31 (2001)

Pojman, J. A., Masere, J., Petretto, E., Rustici, M., Huh, D.-S., Kim, M. S. and Volpert, V.I. The effect of reactor geometry on frontal polymerization spin modes, *Chaos*, 12, 56-65 (2002)

Bazile, M. Jr., Nichols, H. A., Pojman, J. A. and Volpert, Vit. Effect of orientation on thermoset frontal polymerization, *J. Poly. Sci. Part A. Poly. Chem.* 40, 3504-3508 (2002)

Volpert, Vit. A, Pojman, J. A. and Texier-Picard, R. Convection induced by composition gradients in miscible systems, *C. R. Mecanique*, 330, 353-358 (2002).

Pojman, J. A.; Volpert, V. A. and Volpert, V. A "Nonlinear Dynamics of SHS-Like Processes in Polymer Chemistry" in "Self-Propagating High-Temperature Synthesis of Materials." A. A. Borisov, L. T. De Luca, A. G. Merzhanov, eds., Taylor and Francis: New York, 99-118, 2002

Presentations

Ainsworth, W.J. and Pojman, J.A. "Polymeric foam production in frontal polymerization." Presented at the Mississippi Academy of Sciences, Tupelo, Mississippi, February 1999.

Ainsworth, W.J., Pojman, J.A., Warren, J.R., Nguyen, V.V., Wahjudi, P.N., Kendrick, M., and Stewart, F.D. "Polymeric foam experiments in microgravity: results from the NASA KC-135a parabolic flight experiments." Presented at the American Chemical Society, National Meeting, New Orleans, Louisiana, August 1999.

Bazile, M., Nichols, A., and Pojman, J.A. "Orientation dependence of the front velocity of descending thermal fronts." Presented at the Mississippi Academy of Sciences, Tupelo, Mississippi, February 1999.

Chekanov, Y., and Pojman, J.A. "Functionally graded polymeric materials prepared via frontal polymerization." Presented at the Mississippi Academy of Sciences, Tupelo, Mississippi, February 1999.

Chekanov, Y. and Pojman, J.A. "Preparation of gradient materials via frontal polymerization." Presented at the American Chemical Society, National Meeting, New Orleans, Louisiana, August 1999.

Masere, J., Chekanov, Y., and Pojman, J.A. "In situ synthesis of ionic liquid-polymer electrolyte composites by frontal polymerization." Presented at the Mississippi Academy of Sciences, Tupelo, Mississippi, February 1999.

Masere, J., Stewart, F.D., Meehan, T., and Pojman, J.A. "Spin head-doubling behavior in frontal polymerization of multifunctional acrylates." Presented at the American Chemical Society, National Meeting, New Orleans, Louisiana, August 1999.

Pojman, J.A. "Surface tension-induced convection in chemical reaction." Presented at the Mississippi Academy of Sciences, Tupelo, Mississippi, February 1999.

Pojman, J.A. "Frontal polymerization: from microgravity to new materials." Presented at the 5th SIAM Conference on Applications of Dynamical Systems, Snowbird, Utah, May 1999.

Pojman, J.A. "Self organization in synthetic polymeric systems." Presented at the Oscillations and Dynamic Instabilities Gordon Conference, Barca, Italy, May 1999.

Pojman, J.A., and Clarida, W. "An investigation of bubble behavior in viscous frontal polymerization system." Presented at the Mississippi Academy of Sciences, Tupelo, Mississippi, February 1999.

Pojman, J.A., Bazile, M., Dumont, T., Nichols, H.A., and Volpert, V. "The effect of orientation on descending fronts with a solid product." Presented at the Workshop on Modeling Reaction Fronts, Universite Lyon I, Lyon, France, April 1999.

Texier-Picard, R., Pojman, J.A., and Volpert, V. "Effect of interfacial tension on propagating polymerization fronts." Presented at the Workshop on Modeling Reaction Fronts, Universite Lyon I, Lyon, France, April 1999.

Volpert, V., Dumont, T., Chekanov, Y., Masere, J., Wilke, H., and Pojman, J. "The effective interfacial tension in miscible fluids." Presented at the American Chemical Society, National Meeting, New Orleans, Louisiana, August 1999.

Warren, J.R. and Pojman, J.A. "Two-dimensional frontal polymerization." Presented at the American Chemical Society, National Meeting, New Orleans, Louisiana, August 1999.

Pojman, J.A., Volpert, V.A., Dumont, T., Ainsworth, W., Chekanov, Y., Masere, J. "Bubble behavior and convection in frontal polymerization on the KC-135 aircraft." AIAA 2000-0856, presented at the 38th AIAA Aerospace Sciences Meeting, Reno, Nevada, J

Pojman, J.A., Volpert, V.A., Dumont, T., Ainsworth, W., Chekanov, Y., Masere, J. "The effective interfacial tension in miscible fluids." Presented at the Mississippi Academy of Sciences, Biloxi, Mississippi, February 2000.

Pojman, J.A., Volpert, V.A., Dumont, T., Ainsworth, W., Chekanov, Y., Masere, J. "Measuring the effective interfacial tension in miscible fluids by spinning drop tensiometry." Presented at Journes du PSMN, " Mouillage et Tension Superficielle (Wettin

Pojman, J.A., Volpert, V.A., Dumont, T., Ainsworth, W., Chekanov, Y., and Masere, J. "Frontal polymerization in microgravity." Presented at the American Chemical Society National Meeting, San Francisco, California, March 2000.

Pojman, J.A., Volpert, V.A., Dumont, T., Ainsworth, W., Chekanov, Y., and Masere, J. "Frontal polymerization in microgravity: bubble behavior and convection on the KC-135 aircraft." Presented at the 2000 NASA Microgravity Materials Science Meeting, Huntsville, AL

Pojman, J.A., Volpert, V.A., Dumont, T., Ainsworth, W., Chekanov, Y., and Masere, J. "Bubble interactions with frontal polymerization in reduced gravity." Presented at the Gordon Research Conference, Bristol, Rhode Island, August 2000.

Pojman, J.A., Volpert, V.A., Dumont, T., Ainsworth, W., Chekanov, Y., and Masere, J. "Effective interfacial tension induced convection (EITIC) in miscible fluids." Presented at the Gordon Research Conference, Bristol, Rhode Island, August 2000.

Pojman, J. A., Chekanov, Y., Masere, J., Volpert, V., Dumont, T., and Wilke, W. "Effective interfacial tension induced convection (EITIC) in miscible fluids." AIAA-2001-0764, presented at the 39th AIAA Aerospace Sciences Meeting, , Reno, Nevada, January 2001

Pojman, J. A., Chekanov, Y., Masere, J., Volpert, V., Dumont, T., and Wilke, W. "Effective interfacial tension induced convection (EITIC) in miscible fluids." Mississippi Academy of Sciences, Tupelo, Mississippi, February 8-9, 2001

Pojman, J. A., Chekanov, Y., Masere, J., Volpert, V., Dumont, T., and Wilke, W. "Effective interfacial tension induced convection (EITIC) in miscible fluids." International Workshop on Miscible Interfaces, Paris, France, July 2, 2001

Ainsworth, W. and Pojman, J. A. "The use of particle imaging velocimetry to study convection in miscible polymer systems." International Workshop on Miscible Interfaces, Paris, France, July 2, 2001

Volpert, V. "Capillary phenomena in miscible fluids." 8th all Russian Congress in Theoretical and Applied Mechanics, Perm, Russia, August 23-29, 2001

Pojman, J. A., Chekanov, Y., Masere, J., Molden, M., Petteeto, E. and Volpert, V. "Effect of geometry and viscosity on spin modes in frontal polymerization" Pacifichem, Honolulu, HI, December 15, 2000.

Budzinski, K., Carter, N., Leard, K., Watters, C., Zoltowski, B. and Pojman, J. A. "Down to Earth Microgravity Experiments: Classroom Demonstrations of Microgravity Research." AIAA-2002-1114 presented at the 40th AIAA Aerospace Sciences Meeting and Exhibit, 14-17, Reno, Nevada, January 2002.

Bessonov, N., Texier-Picard, R., Volpert, V., Wilke, H., and Pojman, J. A. "Numerical simulations of transient interfacial phenomena in miscible fluids," AIAA-2002-0892 presented at the 40th AIAA Aerospace Sciences Meeting and Exhibit, 14-17, Reno, Nevada, January 2002.

Wilke, H. and Pojman, J. A. "Coupling Between Buoyancy and Marangoni Convection in a Two-Fluid System Under Reduced Gravity: A Numerical Study," AIAA-2002-0756 presented at the 40th AIAA Aerospace Sciences Meeting and Exhibit, 14-17, Reno, Nevada, January 2002.

Ainsworth, W. and Pojman, J. A. "Particle Image Velocimetry as a Method for Measuring Convection in Miscible Polymer Systems," AIAA-02- presented at the 40th AIAA Aerospace Sciences Meeting and Exhibit, 14-17, Reno, Nevada, January 2002.

Bessonov, N., Texier-Picard, R., Volpert, V., Wilke, H., and Pojman, J. A. "Numerical

simulations of transient interfacial phenomena in miscible fluids," Mississippi Academy of Science, Biloxi, MS, February 2002

Pojman, J. A., Bessonov, N., Volpert, V., and Zoltowski, B. "Korteweg stress in miscible systems: a new source of dynamics in reaction-diffusion systems," Gordon Research Conference on "Oscillations & Dynamic Instabilities in Chemical Systems," Queens College, Oxford, UK., July 28 - August 2, 2002

Volpert, Vit. "Instabilities of polymerization fronts," Gordon Research Conference on "Oscillations & Dynamic Instabilities in Chemical Systems," Queens College, Oxford, UK., July 28 - August 2, 2002

Lewis, L. L., DeBisschop, C. A., Pojman, J. A., and Volpert, Vi. "Isothermal frontal polymerization: comparison between modeling and experiment," Gordon Research Conference on "Oscillations & Dynamic Instabilities in Chemical Systems," Queens College, Oxford, UK., July 28 - August 2, 2002

Fortenberry, D., Leard, K., Pojman, J. A. and Volpert, Vit. "Spherically-propagating polymerization fronts," Gordon Research Conference on "Oscillations & Dynamic Instabilities in Chemical Systems," Queens College, Oxford, UK., July 28 - August 2, 2002

Pojman, J. A., Bessonov, N., Texier-Picard, R., Volpert, V., and Wilke, H. "Effective interfacial tension in miscible polymers systems: A possible new source of instabilities," 224th ACS National Meeting, Boston, MA, August 18-22, 2002

Volpert, Vit. and Pojman, J. A. "Binary liquids and diffuse interfaces," Workshop on Patterns and Waves: Theory and Applications, St. Petersburg, Russia, July 8-12, 2002

Lewis, L. L., DeBisschop, C. A., Pojman, J. A., and Volpert, Vi. "Evolution of isothermal polymerization fronts via laser line deflection and predictive modeling," 224th ACS National Meeting, Boston, MA, August 18-22, 2002

Ainsworth, W. and Pojman, J. A. "Measuring convection in miscible polymer using particle image velocimetry," NASA 2002 Materials Science Conference, Huntsville, Alabama, June 25, 2002.

Ainsworth, W. and Pojman, J. A. "Measuring convection in miscible polymer using particle image velocimetry," Mississippi Academy of Science, Biloxi, MS, February 2002

Lewis, L. L. and Pojman, J. A., "Using Laser Line Deflection and shadowgraphy to determine the existence of isothermal frontal polymerization of methyl methacrylate, its front position and its front width," Mississippi Academy of Science, Biloxi, MS, February 2002

Budzinski, K., Carter, N., Leard, K., Zoltowski, B. and Pojman, J. A. "Down to earth microgravity experiments, part I: The benefits of classroom-based drop experiments," Mississippi Academy of Science, Biloxi, MS, February 2002

Budzinski, K., Carter, N., Leard, K., Watters, C., Zoltowski, B. and Pojman, J. A. "Down to earth microgravity experiments, part I: Part II: Verification of plasma behavior in microgravity," Mississippi Academy of Science, Biloxi, MS, February 2002

Leard, K., Tompkins, S., and Pojman, J. A. "Viscosity dependence of spin modes in frontal polymerization of multifunctional acrylates," Mississippi Academy of Science, Biloxi, MS, February 2002

Holloway, R. and Pojman, J. A. "Method for determining viscosity of unknown samples." Roger Holloway and John A. Pojman, Mississippi Academy of Science, Biloxi, MS, February 2002

Lewis, L. L. and Pojman, J. A., "Use of Laser Line Deflection and shadowgraphy as non-invasive monitoring techniques for isothermal frontal polymerization of methyl methacrylate systems," American Chemical Society National Meeting, Orlando, FL, April 7-11, 2002.

Zoltowski, B. and Pojman, J. A. "Spinning Drop Tensiometry of miscible polymer/monomer systems," NASA 2002 Materials Science Conference, Huntsville, Alabama, June 25, 2002.

Pojman, J. A. and Volpert, V. "Convective instabilities in frontal polymerization," J. A. Pojman Sr., V. Volpert, 224th American Chemical Society National Meeting, Boston, MA, August 18-22, 2002.

Patent

Pojman, J. A.; McCardle, T. W. "Functionally Gradient Polymeric Materials," U.S. Patent 6,313,237, 2001.

Pojman, J. A.; McCardle, T. W., "Functionally Gradient Polymeric Materials," 2001, U.S. Patent, Patent No. 6,313,237.

Literature Cited

- 1) Chechilo, N. M.; Khvilivitskii, R. J.; Enikolopyan, N. S. "On the Phenomenon of Polymerization Reaction Spreading," *Dokl. Akad. Nauk SSSR* **1972**, *204*, 1180-1181.
- 2) Chechilo, N. M.; Enikolopyan, N. S. "Effect of the Concentration and Nature of Initiators on the Propagation Process in Polymerization," *Dokl. Phys. Chem.* **1975**, *221*, 392-394.
- 3) Chechilo, N. M.; Enikolopyan, N. S. "Effect of Pressure and Initial Temperature of the Reaction Mixture during Propagation of a Polymerization Reaction," *Dokl. Phys. Chem.* **1976**, *230*, 840-843.
- 4) Davtyan, S. P.; Surkov, N. F.; Rozenberg, B. A.; Enikolopyan, N. S. "Influence of the Gel Effect on the Kinetics of Radical Polymerization under the Conditions of the Polymerization Front Propagation," *Dokl. Phys. Chem.* **1977**, *232*, 64-67.
- 5) Davtyan, S. P.; Gel'man, E. A.; Karyan, A. A.; Tonoyan, A. O.; Enikolopyan, N. S. "Applicability of the Principle of Quasistationary concentrations to the Radical Polymerization of Vinyl monomers under Adiabatic Conditions," *Doklady Phys. Chem.* **1980**, *253*, 579-582.
- 6) Enikolopyan, N. S.; Kozhushner, M. A.; Khanukaev, B. B. "Molecular Weight Distribution during Isothermal and Frontal Polymerization," *Doklady Phys. Chem.* **1974**, *217*, 676-678.
- 7) Khanukaev, B. B.; Kozhushner, M. A.; Enikolopyan, N. S. "Theory of the Propagation of a Polymerization Front," *Dokl. Phys. Chem.* **1974**, *214*, 84-87.
- 8) Khanukaev, B. B.; Kozhushner, M. A.; Enikolopyan, N. S. "Theory of Polymerization-Front Propagation," *Combust. Explos. Shock Waves* **1974**, *10*, 562-568.
- 9) Surkov, N. F.; Davtyan, S. P.; Rozenberg, B. A.; Enikolopyan, N. S. "Calculation of the Steady Velocity of the Reaction Front during Hardening of Epoxy Oligomers by Diamines," *Dokl. Phys. Chem.* **1976**, *228*, 435-438.
- 10) Arutyunyan, K. A.; Davtyan, S. P.; Rozenberg, B. A.; Yenikolopyan, N. S. "Kinetics of Adiabatic Thermal Setting of Oligo-Epoxydianes in the Presence of m-Phenylenediamine," *Polymer Science USSR* **1975**, *17*, 333-338.
- 11) Pojman, J. A. "Traveling Fronts of Methacrylic Acid Polymerization," *J. Am. Chem. Soc.* **1991**, *113*, 6284-6286.
- 12) Pojman, J. A.; Craven, R.; Khan, A.; West, W. "Convective Instabilities In Traveling Fronts of Addition Polymerization," *J. Phys. Chem.* **1992**, *96*, 7466-7472.
- 13) Pojman, J. A.; Willis, J.; Fortenberry, D.; Ilyashenko, V.; Khan, A. "Factors Affecting Propagating Fronts of Addition Polymerization: Velocity, Front Curvature, Temperature Profile, Conversion and Molecular Weight Distribution," *J. Polym. Sci. Part A: Polym Chem.* **1995**, *33*, 643-652.
- 14) Pojman, J. A.; Nagy, I. P.; Salter, C. "Traveling Fronts of Addition Polymerization with a Solid Monomer," *J. Am. Chem. Soc.* **1993**, *115*, 11044-11045.
- 15) Pojman, J. A.; Ilyashenko, V. M.; Khan, A. M. "Free-Radical Frontal Polymerization: Self-Propagating Thermal Reaction Waves," *J. Chem. Soc. Faraday Trans.* **1996**, *92*, 2825-2837.
- 16) Khan, A. M.; Pojman, J. A. "The Use of Frontal Polymerization in Polymer Synthesis," *Trends Polym. Sci. (Cambridge, U.K.)* **1996**, *4*, 253-257.

- 17) Pojman, J. A.; Khan, A. M.; West, W. "Traveling Fronts Of Addition Polymerization: A Possible New Method Of Materials Synthesis.," *Polym. Prepr. (Am Chem. Soc. Div. Polym. Chem.)* **1992**, 33, 1188-1189.
- 18) Chechilo, N. M.; Enikolopyan, N. S. "Structure of the Polymerization Wave Front and Propagation Mechanism of the Polymerization Reaction," *Dokl. Phys. Chem.* **1974**, 214, 174-176.
- 19) Garbey, M.; Taik, A.; Volpert, V. "Influence of Natural Convection on Stability of Reaction Fronts in Liquids," *Quart. Appl. Math.* **1998**, 56, 1-35.
- 20) Garbey, M.; Taik, A.; Volpert, V. "Influence of Natural Convection on Stability of Reaction Fronts in Liquids," *Preprint CNRS* **1994**, 187, 1-42.
- 21) Garbey, M.; Taik, A.; Volpert, V. "Linear Stability Analysis of Reaction Fronts in Liquids," *Quart. Appl. Math.* **1996**, 54, 225-247.
- 22) Bowden, G.; Garbey, M.; Ilyashenko, V. M.; Pojman, J. A.; Solovyov, S.; Taik, A.; Volpert, V. "The Effect of Convection on a Propagating Front with a Solid Product: Comparison of Theory and Experiments," *J. Phys. Chem. B* **1997**, 101, 678-686.
- 23) Pojman, J. A.; Epstein, I. R. "Convective Effects on Chemical Waves. 1. Mechanisms and Stability Criteria.," *J. Phys. Chem.* **1990**, 94, 4966-4972.
- 24) Pojman, J. A.; Epstein, I. R.; McManus, T.; Showalter, K. "Convective Effects on Chemical Waves. 2. Simple Convection in the Iodate-Arsenous Acid System," *J. Phys. Chem.* **1991**, 95, 1299-1306.
- 25) Pojman, J. A.; Epstein, I. R.; Nagy, I. "Convective Effects on Chemical Waves. 3. Multicomponent Convection in the Iron(II)-Nitric Acid System," *J. Phys. Chem.* **1991**, 95, 1306-1311.
- 26) Masere, J.; Vasquez, D. A.; Edwards, B. F.; Wilder, J. W.; Showalter, K. "Nonaxisymmetric and Axisymmetric Convection in Propagating Reaction-Diffusion Fronts," *J. Phys. Chem.* **1994**, 98, 6505-6508.
- 27) Plesser, T.; Wilke, H.; Winters, K. H. "Interaction of Chemical Waves with Convective Flows Induced by Density Gradients. A Comparison Between Experiments and Computer Simulations," *Chem. Phys. Lett.* **1992**, 200, 158-162.
- 28) Wu, Y.; Vasquez, D. A.; Edwards, B. F.; Wilder, J. W. "Convective Chemical-Wave Propagation in the Belousov-Zhabotinsky Reaction," *Phys. Rev. E* **1995**, 51, 1119-1127.
- 29) Goldfeder, P. M.; Volpert, V. A.; Ilyashenko, V. M.; Khan, A. M.; Pojman, J. A.; Solovyov, S. E. "Mathematical Modeling of Free-Radical Polymerization Fronts," *J. Phys. Chem. B* **1997**, 101, 3474-3482.
- 30) Pojman, J. A.; Gunn, G.; Owens, J.; Simmons, C. "Frontal Dispersion Polymerization," *J. Phys. Chem. Part B* **1998**, 102, 3927-3929.
- 31) McCaughey, B.; Pojman, J. A.; Simmons, C.; Volpert, V. A. "The Effect of Convection on a Propagating Front with a Liquid Product: Comparison of Theory and Experiments," *Chaos* **1998**, 8, 520-529.
- 32) Pojman, J. A.; McCardle, T. W., "Functionally Gradient Polymeric Materials," 2000, U.S. Patent, Patent No. 6,057,406.
- 33) Pojman, J. A.; McCardle, T. W., "Functionally Gradient Polymeric Materials," 2001, U.S. Patent, Patent No. 6,313,237.
- 34) Chekanov, Y. A.; Pojman, J. A. "Preparation of Functionally Gradient Materials Via Frontal Polymerization," *J. Appl. Polym. Sci.* **2000**, 78, 2398-2404.

- 35) Bazile Jr., M.; Nichols, H. A.; Pojman, J. A.; Volpert, V. "The Effect of Orientation on Thermoset Frontal Polymerization," *J. Polym. Sci. Part A: Polym Chem.* **2002**, *40*, 3504-3508.
- 36) Maksimov, Y. M.; Pak, A. T.; Lavrenchuk, G. V.; Naiborodenko, Y. S.; Merzhanov, A. G. "Spin combustion of gasless systems," *Comb. Expl. Shock Waves* **1979**, *15*, 415-418.
- 37) Begishev, V. P.; Volpert, V. A.; Davtyan, S. P.; Malkin, A. Y. "On some Features of the Process of Anionic Activated Polymerization of ϵ -caprolactans under Conditions of Wave Propagation," *Dokl. Akad. Nauk SSSR* **1973**, *208*, 892.
- 38) Begishev, V. P.; Volpert, V. A.; Davtyan, S. P.; Malkin, A. Y. "On some Features of the Anionic Activated ϵ -Caprolactam Polymerization Process under Wave Propagation Conditions," *Dokl. Phys. Chem.* **1985**, *279*, 1075-1077.
- 39) Pojman, J. A.; Ilyashenko, V. M.; Khan, A. M. "Spin Mode Instabilities in Propagating Fronts of Polymerization," *Physica D* **1995**, *84*, 260-268.
- 40) Ilyashenko, V. M.; Pojman, J. A. "Single Head Spin Modes in Frontal Polymerization," *Chaos* **1998**, *8*, 285-287.
- 41) Masere, J.; Stewart, F.; Meehan, T.; Pojman, J. A. "Period-Doubling Behavior in Propagating Polymerization Fronts of Multifunctional Acrylates," *Chaos* **1999**, *9*, 315-322.
- 42) Pojman, J. A.; Masere, J.; Petretto, E.; Rustici, M.; Huh, D.-S.; Kim, M. S.; Volpert, V. "The Effect of Reactor Geometry on Frontal Polymerization Spin Modes," *Chaos* **2002**, *12*, 56-65.
- 43) Masere, J.; Chekanov, Y.; Warren, J. R.; Stewart, F.; Al-Kaysi, R.; Rasmussen, J. K.; Pojman, J. A. "Gas-Free Initiators for High-Temperature Polymerization," *J. Poly. Sci. Part A. Polym. Chem.* **2000**, *38*, 3984-3990.
- 44) Texier-Picard, R.; Pojman, J. A.; Volpert, V. A. "Effect of Interfacial Tension on Propagating Polymerization Fronts," *Chaos* **2000**, *10*, 224-230.
- 45) Volpert, V. A.; Volpert, V. A.; Pojman, J. A. "Effect of Thermal Expansion on Stability of Reaction Front Propagation," *Chem. Eng. Sci.* **1994**, *14*, 2385-2388.
- 46) Bruins, F. P. *Polyurethane Technology*; Bruins, F. P.; Wiley-Interscience: New York, 1969.
- 47) Saunders, J. H.; Frisch, K. C. *Polyurethanes: Chemistry and Technology, Part 1, Chemistry*"; Wiley-Interscience, New York: 1962.
- 48) Khemani, K. C. *Polymeric foams: science and technology*; Khemani, K. C.; American Chemical Society: Washington, D.C., 1997.
- 49) Wessling, F. C.; Maybee, G. W. "Consort 1 Sounding Rocket Flight," *Journal of Spacecraft and Rockets* **1989**, *26*, 343-351.
- 50) Wessling, F. C.; McManus, S. P.; Matthews, J.; Patel, D. "Foam Formation in Low Gravity," *J. Spacecraft and Rockets* **1990**, *27*, 324-329.
- 51) Bergman, A.; Frederikson, H.; Shahani, H. *J. Mat. Sci.* **1998**, *23*, 1573-1579.
- 52) Curtin, M. M.; Tyler, F. S.; Wilkinson, D. "Polymer Foam Cell Growth in Microgravity," *J. Cell. Plastics* **1992**, *28*, 536-556.
- 53) Pojman, J. A.; Khan, A. M.; Mathias, L. J. "Frontal Polymerization in Microgravity: Results from the *Conquest I* Sounding Rocket Flight," *Microgravity sci. technol.* **1997**, *X*, 36-40.
- 54) Pojman, J. A.; Khan, A. M.; Mathias, L. "Frontal Polymerization in Microgravity," *Polym. Prepr. (Am Chem. Soc. Div. Polym. Chem.)* **1997**, *38(1)*, 717-718.
- 55) Pojman, J. A., Frontal Polymerization in Microgravity, AIAA 98-08113, *36th Aerospace Sciences Meeting*, **1998**,

- 56) Pojman, J.; Volpert, V.; Dumont, T.; Ainsworth, W.; Chekanov, Y.; Masere, J.; Wilke, H., Bubble Behavior and Convection in Frontal Polymerization on the KC-135 Aircraft, AIAA 2000-0856, 38th Aerospace Sciences Meeting, 2000,
- 57) Chekanov, Y.; Pojman, J. A.; Rasmussen, J. K. "Bubble-Free Initiators for High Temperature Free-Radical Polymerization," *Polym. Prepr. (Am Chem. Soc. Div. Polym. Chem.)* **1998**, 39, 465-467.
- 58) Balasubramaniam, R.; Lacy, C. E.; Woniak, G.; Subramanian, R. S. "Thermocapillary Migration of Bubbles and Drops at Moderate Values of the Marangoni Number in Reduced Gravity," *Phys. Fluids* **1996**, 8, 872-880.
- 59) Probstein, R. F. *Physicochemical Hydrodynamics.*; Wiley: New York, 1994.
- 60) Petitjeans, P.; Maxworthy, T. "Miscible displacements in capillary tubes. Part 1. Experiments," *J. Fluid Mech.* **1996**, 326, 37-56.
- 61) Cahn, J. W.; Hilliard, J. E. "Free Energy of a Nonuniform System. I. Interfacial Free Energy," *J. Chem. Phys.* **1958**, 28, 258-267.
- 62) Rousar, I.; Nauman, E. B. "A Continuum Analysis of Surface Tension in Nonequilibrium Systems," *Chem. Eng. Comm.* **1994**, 129, 19-28.
- 63) Korteweg, D. J. "Sur la forme que prennent les quations du mouvements des fluides si l'on tient compte des forces capillaires causes par des variations de densit considrables mais coninues et sur la thorie de la capillarit dans l'hypothse d'une variation continue de la densit," *Archives Néerlandaises des Sciences Exactes et Naturelles* **1901**, 6, 1-24.
- 64) Anderson, D. M.; McFadden, G. B.; Wheeler, A. A. "Diffuse-Interface Methods in Fluids Mechanics," *Ann. Rev. Fluid Mech* **1998**, 30, 139-165.
- 65) van der Waals, J. D. "The Thermodynamic Theory of Capillarity under the Hypothesis of a Continuous Variation in Density (translated by J. Rowlinson)," *J. Stat. Phys.* **1979**, 20, 197-244.
- 66) Yang, A. J. M.; Fleming III, P. D.; Gibbs, J. H. "Molecular Theory of Surface Tension," *J. Chem. Phys.* **1976**, 64, 3732-3747.
- 67) Antanovskii, L. K. "A phase field model of Capillarity," *Phys. Fluids* **1995**, 7, 747-753.
- 68) Jacqmin, D. "Contact-line Dynamics of a Diffuse Fluid Interface," *J. Fluid Mech.* **2000**, 402, 57-88.
- 69) Jacqmin, D. "Calculation of Two-Phase Navier-Stokes Flows Using Phase-field Modeling," *J. Comput. Phys.* **1999**, 155, 96-127.
- 70) Jasnow, D.; Vials, J. "Course-Grained Description of Thermo-capillary Flows," *Phys. Fluids* **1996**, 8, 660-669.
- 71) Anderson, D. M.; McFadden, G. B. "A Diffuse-interface Description of Internal Waves in a Near-critical Fluid," *Phys. Fluids* **1997**, 9, 1870-1879.
- 72) Joseph, D. D.; Renardy, Y. Y. *Fundamentals of Two-Fluid Dynamics. Part II. Lubricated Transport, Drops and Miscible Fluids*; Springer: New York, 1992.
- 73) May, S. E.; Maher, J. V. "Capillary-Wave Relaxation for a Meniscus between Miscible Liquids," *Phys. Rev. Ltt.* **1991**, 67, 2013-2015.
- 74) Garik, P.; Hetrick, J.; Orr, B.; Barkey, D.; Ben-Jacob, E. "Interfacial Cellular Mixing and a Conjecture on Global Deposit Morphology," *Phys. Rev. Ltt* **1991**, 66, 1606-1609.
- 75) Ma, W. J.; Kebllinski, P.; Maritan, A.; Koplik, J.; Banavar, J. R. "Dynamical Relaxation of the Surface Tension of Miscible Phases," *Phys. Rev. Ltt.* **1993**, 71, 3465-3468.
- 76) Mungall, J. E. "Interfacial Tension in Miscible Two-Fluid Systems with Linear Viscoelastic Rheology," *Phys. Rev. Ltt.* **1994**, 73, 288-291.

- 77) Castellanos, A.; Gonzalez, A. "Interfacial Electrohydrodynamic Instability: The Kath and Hoburg Model Revisited," *Phys. Fluids A* **1992**, *4*, 1307-1309.
- 78) Vonnegut, B. "Rotating Bubble Method for the Determination of Surface and Interfacial Tensions," *Rev. Sci. Instrum.* **1942**, *13*, 6-9.
- 79) Hu, H. H.; Joseph, D. D. "Evolution of a Liquid Drop in a Spinning Drop Tensiometer," *J. Colloid Interface Sci.* **1994**, *162*, 331-339.
- 80) Heinrich, M.; Wolf, B. A. "Establishment of Phase Equilibria: Temperature Jump Experiments in a Spinning-Drop Apparatus," *Macromolecules* **1993**, *26*, 6106-6110.
- 81) Petitjeans, P. "Une Tension de Surface pour les Fluides Miscibles," *C.R. Acad. Sci. Paris* **1996**, *322*, 673-679.
- 82) Bessonov, N. M.; Song, D. J. "Application of Vector Calculus to Numerical Solutions of Continuum Mechanics Problems," *J. Comp. Phys.* **2001**, *167*, 22-38.
- 83) Volpert, V. A.; Pojman, J. A.; Texier-Picard, R. "Convection Induced by Composition Gradients in Miscible Systems," *C. R. Mecanique* **2002**, *330*, 353-358.
- 84) Pojman, J.; Volpert, V.; Dumont, T.; Chekanov, Y.; Masere, J.; Wilke, H., Effective Interfacial Tension Induced Convection (EITIC) in miscible fluids, *AIAA 2001-0764, 39th Aerospace Sciences Meeting*, **2001**,
- 85) Joseph, D. D.; Arney, M. S.; Gillber, G.; Hu, H.; Hultman, D.; Verdier, C.; Vinagre, T. M. "A Spinning Drop Tensioextensometer," *Journal of Rheology* **1992**, *36*, 621-662.
- 86) Joseph, D. D. "Upper and Lower Bounds for Interfacial Tension Using Spinning Drop Devices," *Journal of Colloid and Interface Science* **1992**, *148*, 291-294.
- 87) Currie, P. K.; Van Nieuwkoop, J. "Buoyancy Effects in the Spinning-Drop Interfacial Tensiometer," *J. Colloid Interface Sci.* **1982**, *87*, 301-316.
- 88) Princen, H. M.; Zia, I. Y. Z.; Mason, S. G. "Measurement of Interfacial Tension from the Shape of a Rotating Drop," *J. Colloid and Inter. Sci.* **1967**, *23*, 99-107.
- 89) Slattery, J. C. C., Jing-Den "Notes: Alternative Solution for Spinning Drop Interfacial Tensiometer," *Journal of Colloid and Interfacial Science* **1978**, *64*, 371-373.
- 90) McMaster, L. P. Copolymer, Polyblends, and Composites: in Platzner, N. A., Ed.; American Chemical Society: Washington D.C., 1975; pp 43-65.
- 91) Valdes-Aguilera, O.; Pathak, C. P.; Neckers, D. C. "Pyrene as a Fluorescent Probe for Monitoring Polymerization Rates," *Macromolecules* **1990**, *23*, 689-692.
- 92) Vatanparast, R.; Le, S.; Hakala, K.; Lemmetyinen, H. "Monitoring of Curing of Polyurethane Polymers with a Fluorescence Method," *Macromolecules* **2000**, *33*, 438-443.
- 93) Paczkowski, J.; Neckers, D. C. "Following Polymerization Kinetics of Multifunctional Acrylates in Real Time by Fluorescence Probe Methodology," *Macromolecules* **1992**, *25*, 548-553.
- 94) Paczkowski, J.; Neckers, D. C. "New Fluorescence Probes for Monitoring the Kinetics of Laser-Initiated Polymerization," *J. Polym. Sci. Part A: Polym Chem.* **1993**, *31*, 841-846.
- 95) Jager, W. F.; Volkers, A. A.; Neckers, D. C. "Solvatochromic Fluorescent Probes for Monitoring the Photopolymerization of Dimethacrylates," *Macromolecules* **1995**, *28*, 8153-8158.
- 96) Migler, K. B.; Bur, A. J. "Fluorescence Based Measurement of Temperature Profiles During Polymer Processing," *Polym. Eng. Sci.* **1998**, *38*, 213-221.